

4-2012

Heart Rate Artifact Suppression

Christopher Dickson
Grand Valley State University

Follow this and additional works at: <https://scholarworks.gvsu.edu/theses>

ScholarWorks Citation

Dickson, Christopher, "Heart Rate Artifact Suppression" (2012). *Masters Theses*. 18.
<https://scholarworks.gvsu.edu/theses/18>

This Thesis is brought to you for free and open access by the Graduate Research and Creative Practice at ScholarWorks@GVSU. It has been accepted for inclusion in Masters Theses by an authorized administrator of ScholarWorks@GVSU. For more information, please contact scholarworks@gvsu.edu.

Heart Rate Artifact Suppression

Author: Christopher Dickson

A Thesis Submitted to the Graduate Faculty of

GRAND VALLEY STATE UNIVERSITY

In

Partial Fulfillment of Requirements

For the Degree of

Master of Science in Engineering with a Biomedical Emphasis

Padnos College of Engineering and Computing

April 2012

Acknowledgements

I would like to acknowledge the School of Engineering and my advisor Dr. Samhita Rhodes, and Dr. Bruce Dunne for their continued support during this thesis. I would also like to thank Twistthink, LLC and Warren Guthrie for their continued support and for giving me the opportunity to work on this project. The completion of this work would not have been possible without them. I am deeply grateful. This project was funded under the National Science Foundation American Recovery and Reinvestment Act of 2009 (ARRA) (Public Law 111-5).

Abstract

Motion artifact strongly corrupts heart rate measurements in current pulse oximetry systems. In many, almost any motion will greatly diminish the system's ability to extract a reliable heart rate. The artifact is most likely present due to normally non-pulsatile components of the body, such as venous blood and tissue fluid, which become pulsatile during motion. This paper presents a motion artifact reduction method using an accelerometer that attempts to recover a usable heart rate sensor signal that has been corrupted by motion. The method was developed for a wrist pulse oximeter sensor and was adapted for a ring sensor, both of which were very susceptible to arm motion. An accelerometer was paired with the pulse oximeter to detect the motion. This motion signal was then used to recover the corrupted heart rate signal. The correlation between the acceleration and the heart rate signals was analyzed and two adaptive filter models were created to relate the corrupted signal to the acceleration. These filters were partially successful in removing the motion artifact. The results show that the wrist sensor was much more susceptible to motion in any direction, while the ring sensor was mainly susceptible to motion in the same direction as the digital artery.

Table of Contents

Acknowledgements.....	iii
Abstract.....	iv
1 Introduction	1
2 Background	2
2.1 History of Oximetry and Pulse Oximetry	2
2.2 Oximetry.....	2
2.3 Principle of Pulse Oximetry	2
2.4 Oxygen Saturation Calculation	5
2.5 Heart Rate Calculation	6
2.6 Modes of Pulse Oximetry.....	6
2.7 Sensor Placement	7
2.8 Applications of Pulse Oximetry	8
2.9 Basic Assumptions of Pulse Oximetry.....	8
2.10 Limitations of Pulse Oximetry	9
2.11 Motion Artifact.....	10
2.12 Current Device Features.....	12

2.13	Products Currently on the Market: Heart Rate Monitoring Watches.....	13
2.14	Current Techniques to Reduce Motion Artifact.....	16
2.14.1	Hardware.....	16
2.14.2	Software.....	16
2.15	Filtering Techniques.....	20
2.15.1	Adaptive Filtering.....	20
2.15.2	Wiener Filtering.....	21
2.15.3	Kalman Filtering.....	22
2.15.4	Wigner-Ville Distribution.....	23
2.15.5	Wavelet Transform.....	23
2.15.6	Weighted Moving Average.....	24
3	Specific Aims.....	25
4	Methods.....	27
4.1	Integrated Pulse Oximeter and Accelerometer Wrist and Finger Sensor.....	27
4.2	Data Gathering.....	27
4.3	Additive Distortion Model.....	30
4.4	Correlation Analysis.....	30
4.5	Adaptive Filter Model.....	34

4.5.1	Least Mean Squares Adaptive Filter.....	35
4.5.2	Recursive Least Squares Adaptive Filter.....	35
4.5.3	Model Assumptions	36
4.5.4	Filter Resolution.....	37
5	Results	38
5.1	Data Collection Analysis.....	38
5.2	Correlation Analysis.....	41
5.3	Adaptive Filter Results.....	43
5.3.1	Wrist Sensor Filter Results	43
5.3.2	Ring Sensor Filter Results	49
5.3.3	Wrist Sensor and Ring Sensor Comparison.....	54
6	Discussion and Conclusion	56
6.1	Correlation.....	56
6.2	Filtering	56
6.3	Future Work	58
7	Works Cited.....	60
	Appendix A: MATLAB Code	62

FIGURES

Figure 2-1: Transmitted Light Absorbance Coefficients for Different Hemoglobin Species (4).....	4
Figure 2-2: Components of Light Absorption By Material In Pulse Oximetry (4)	4
Figure 2-3: LED and Photodetector placement for transmission mode (5).....	7
Figure 2-4: LED and Photodetector placement for reflectance mode (5).....	7
Figure 2-5: Sensor displacement altering backscattered light (5). (A) Typical light scattering before motion, (B) motion induced cyclical movement causes changes in sensor position, changing the backscattered light.	12
Figure 2-6: Example of a heart rate monitoring watch using a chest strap.....	14
Figure 2-7: ePulse2 watch that uses chest strap technology on the arm.....	14
Figure 2-8: Example of heart rate monitoring watch using two fingers to extract a heart rate.....	15
Figure 2-9: AquaPulse Heart Rate Monitor using infrared sensor at the ear lobe	15
Figure 2-10: Adaptive Filter Block Diagram (17)	21
Figure 2-11: Wiener Filter Block Diagram.....	22
Figure 2-12: Kalman Filter Block Diagram.....	22
Figure 2-13: Wavelet Transform Block Diagram.....	24
Figure 4-1: Prototype with integrated accelerometer and heart rate detector	27
Figure 4-2: Results from motion: The top plot is the corrupted heart rate signal and the bottom plot is the z-axis of the accelerometer	29
Figure 4-3: Screen capture of the user interface used to collect the signals	29
Figure 4-4: Block diagram of the additive distortion model adaptive filter	30
Figure 4-5: Comparison of heart rate signals from opposite arms.....	33

Figure 4-6: Subtraction of heart rates from the left and right arm.....	33
Figure 5-1: Vascular anatomy of the arm and hand.....	38
Figure 5-2: Motion corruption on the wrist in the x-axis.....	39
Figure 5-3: Motion corruption at the wrist on the y-axis.....	39
Figure 5-4: Motion corruption on the wrist on the z-axis.....	40
Figure 5-5: A lack of motion corruption at the ring finger despite significant motion on the x-axis.....	40
Figure 5-6: Motion corruption in the axis parallel to the digital artery at the ring finger	41
Figure 5-7: Example of a correlation output.....	43
Figure 5-8: The original 5 second window that is going to be filtered.....	44
Figure 5-9: LMS Output signal vs. Accelerometer Signal	45
Figure 5-10: LMS Filter Error signal compared to the original heart rate signal and the reference heart rate signal	46
Figure 5-11: RLS output signal vs. the original accelerometer signal.....	47
Figure 5-12: RLS Adaptive filter error output vs. the heart rate signals	47
Figure 5-13: Power spectrum of the signals	48
Figure 5-14: Original 5 second window for the ring sensor	49
Figure 5-15: LMS output signal vs. original accelerometer signal.....	50
Figure 5-16: LMS filter error signal compared to the original corrupted heart rate signal	51
Figure 5-17: RLS output signal vs. the original accelerometer signal.....	52
Figure 5-18: RLS filter error signal compared to the original corrupted heart rate signal	53
Figure 5-19: Power spectrum of the signals	54

TABLES

Table 5-1: Correlation data for the wrist data sets: Averages (include standard errors)	42
Table 5-2: Correlation data for the ring finger data sets: Averages.....	42
Table 5-3: Data Summary for LMS and RLS filters across the wrist and ring sensors.....	55

1 INTRODUCTION

Pulse oximetry is a technique that is used to non-invasively monitor both arterial oxygen saturation and heart rate (1). It is widely used in clinics and hospitals throughout the world, mainly because it has the ability to monitor several physiological signals that are of great use when monitoring a patient, including oxygen saturation, heart rate, heart rate variability, and respiration rate. While it is widely used, it does suffer from some serious limitations. The most severe is likely its susceptibility to motion artifact which is the reason that it is most useful in patients with limited mobility. For this project, we will investigate the ability to use pulse oximetry to obtain accurate heart rate information in mobile patients using a device designed by Twistthink, LLC for AFrame Digital: the heart rate watch.

This pre-existing watch monitors patients for falls using an on-board accelerometer. The company wanted to augment its functionality by incorporating a heart rate measurement using pulse-oximetry without the need for an accessory attachment, such as a finger sensor. In essence, it would be the first single electrode, unipolar, estimate of heart rate, which is usually estimated using a differential signal necessitating bipolar electrodes. This led to the use of flex strips that contains light emitting diodes (LEDs) and photodiodes connected to the main watch. The design has resulted in an ability to obtain a heart rate in a patient that is relatively still but it is very susceptible to motion artifact.

Notionally, motion of the limb associated with the measuring circuit should correlate with the interference. This leads to the thought that by sensing the motion of the arm that is wearing the circuit, it should be possible to adaptively cancel the motion artifact. Preliminary techniques yielded mixed results. The accelerometer data was streamed along with the heart rate signal. These signals were then analyzed using Matlab's Simulink Software. Several different filtering methods were employed, none of which resulted in a very clean heart rate signal. These methods were all digital and included low pass filters, Least Mean Squares (LMS) adaptive filters and a matched filter. These techniques were performed on whole signals, rather than windows of motion corruption. It was confirmed that the accelerometer signal, resulting from motion of the arm, did correlate to the heart rate signal but none of the filters were successful at producing a clean enough signal to reliably extract a heart rate. This research will further explore the use of accelerometer signals being used to cancel motion artifact, while also potentially incorporating other methods for cancellation, such as Kalman filtering and wavelet analysis. All of these techniques are commonly used to filter physiological signals, especially electrocardiograms (ECG). If successful, a product using the filtering technique described could be of great value to not only hospitals but also athletes, and the general public, who want to have the ability to continuously monitor key vital signs even while exercising or moving that may be incorporated into a simple device with a single electrode. Heart rate and heart rate variability could play a major role in the prevention and detection of overtraining in athletes.

2 BACKGROUND

2.1 History of Oximetry and Pulse Oximetry

Photoplethysmography (PPG), more commonly known as pulse oximetry, is a way of monitoring vital body signs such as heart rate and blood oxygenation (SpO_2). A pulse oximeter is a medical device that indirectly monitors oxygen saturation and changes in blood volume, generally from a finger or ear lobe. The modern, portable pulse oximeter is used in almost every hospital and can be purchased at many stores worldwide.

2.2 Oximetry

Oximetry is the measurement of percent saturation of oxygen in hemoglobin and is directly correlated with the partial pressure of oxygen in hemoglobin (2). Hemoglobin is a protein that carries oxygen from the lungs to the tissues and is transported by red blood cells (3). This partial pressure of hemoglobin determines how well oxygen is delivered to the cell tissue (2). The basic concept is to transmit light through blood and have the blood absorb a certain amount of light depending on the concentration of oxygenated and deoxygenated hemoglobin (2).

2.3 Principle of Pulse Oximetry

Pulse oximeters are used to non-invasively monitor both arterial oxygen saturation and heart rate (1). These values are calculated based on the transmission, absorption and dispersion of light as it passes through hemoglobin (2). This principle is based on the different light absorbing characteristics of oxyhemoglobin (HbO_2) and deoxyhemoglobin (reduced hemoglobin, Hb) at two different wavelengths, red and infrared and relies on the

pulsatile nature of arterial blood flow (4). These characteristics are shown in Figure 2-1 (4) and Figure 2-2 (4). In Figure 2-1, the different extinction coefficients are shown for the different types of hemoglobin. These extinction coefficients are representative of the absorption coefficients that will have a major role in determining how much light is absorbed. Figure 2-2 shows how the two different light components, as described earlier, are divided (4). This indicates that the AC signal of the pulsing arterial blood sits on top of a DC component that is composed of venous blood, bone, fat, muscle, and other body tissues (4). Component A is the transmitted light intensity that occurs during systole, which is contraction of the heart, and is a result of pulsations of oxygenated arterial blood (4). Component B is transmitted light during diastole. This means that component A can be used to determine the heart rate of the patient, as it coincides with the heart beat because the arterial blood vessels expand and contract with each heart beat (3). With each heartbeat, a new surge of blood fills the arteries to carry more hemoglobin and oxygen to the peripheral tissues and will result in a spike in the oximetry signal, as more blood is present during the transmission of the light (3).

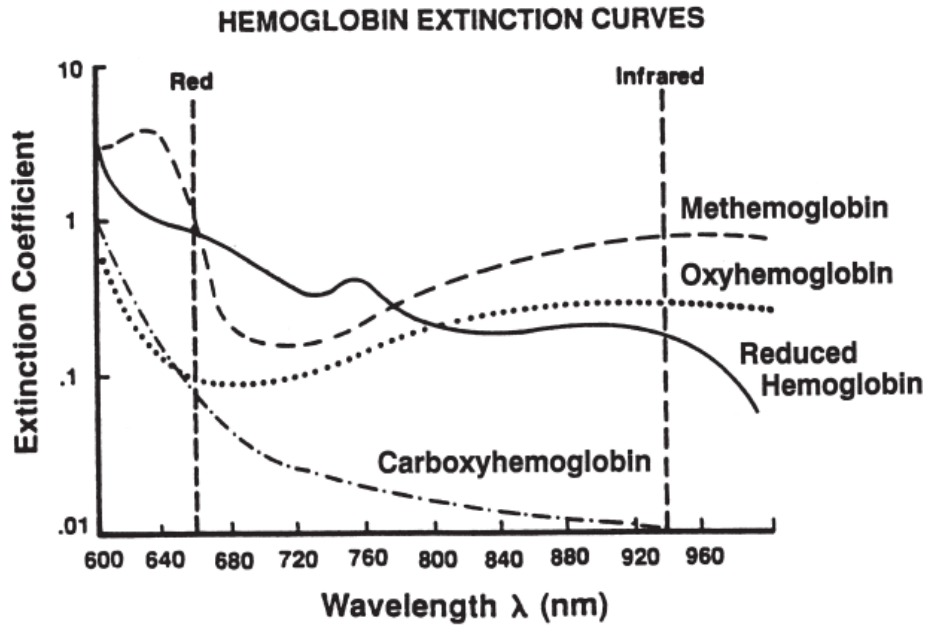


Figure 2-1: Transmitted Light Absorbance Coefficients for Different Hemoglobin Species (4)

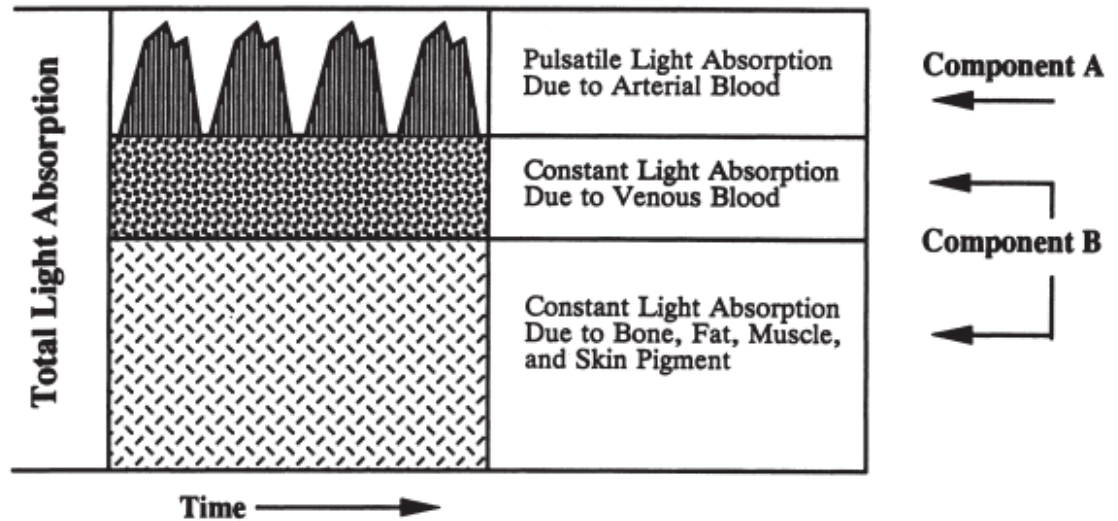


Figure 2-2: Components of Light Absorption By Material In Pulse Oximetry (4)

In most systems, two light emitting diodes (LEDs) at two different wavelengths, red and infrared, are used in conjunction with a photodetector that transduces the light intensity into an electrical signal. It is the different levels of absorption at these two wavelengths, along with pulsatile changes, that provides the information necessary to determine the oxygen saturation and calculate the heart rate (1). The red to infrared ratio is calculated and then compared to a table that consists of empirical formulas that convert the ratio to an oxygen saturation value (5). As mentioned previously, the pulsing of the light transmission due to changing arterial blood volume is used to calculate the heart rate. The magnitude of the signal is a function of the amount of blood that is ejected from the heart during systole, the light absorption of the blood and other components, and the wavelengths used to transmit the light (5). During diastole, the volume of blood in the vascular tissue bed is decreased, which increases the amount of light that is transmitted through (5). This period is the rising portion of the signal (5). During systole, this volume increases causing more light to be absorbed and reducing the intensity of the light measured by the photodetector (5).

2.4 Oxygen Saturation Calculation

The pulse oximeter signal consists of two components: a pulsatile part, referred to as the AC component, and a non-pulsatile part, referred to as the DC component. This DC component is due to light absorption by skin, tissue, venous blood, bone, and non-pulsatile arterial blood. The AC component is caused by light absorption of pulsatile arterial blood.

2.5 Heart Rate Calculation

There are two different methods that are commonly used to extract the heart rate from the PPG signal, peak to peak intervals and monitoring the frequency content. The first method identifies the peaks of the PPG signal and calculates the time between each one. The heart rate is the reciprocal of this time. The second method identifies the frequency of the pulses through the use of a transform, such as the Fourier Transform. This transform will yield a large spike at the frequency of the heart rate.

2.6 Modes of Pulse Oximetry

Pulse oximeters operate in two different ways, with transmission and reflectance (5). In transmission, shown in Figure 2-3, the light sources are on the opposite side of the photodetector. In this scenario, the light is transmitted through the medium and detected on the other side. In reflectance, shown in Figure 2-4, the photodetectors and LEDs are located on the same side of the medium. The photodetector will detect the light that is back-scattered off the tissue, bones, arterial blood, and venous blood. Reflectance will be the method used in this study.

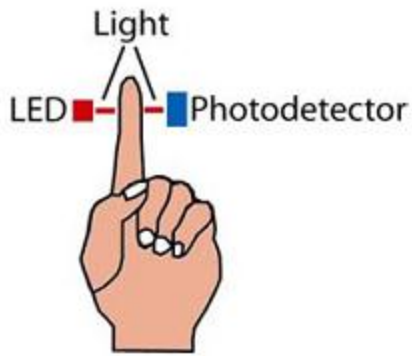


Figure 2-3: LED and Photodetector placement for transmission mode (5)

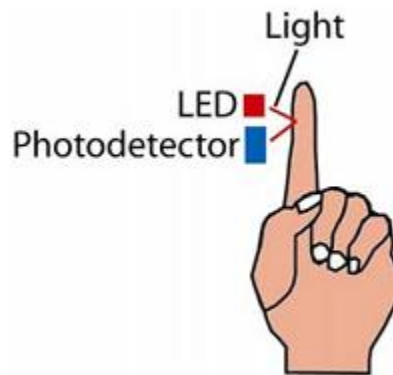


Figure 2-4: LED and Photodetector placement for reflectance mode (5)

2.7 Sensor Placement

The concept of pulse oximetry began with measurements being taken at the ear until Aoyagi discovered the same basic principles could be used at the finger (6). While the finger is still the most common location for the sensors, there are numerous other locations pulse oximeters can be placed. These locations include the chest, cheek, and forehead (5). This study will focus on two locations not commonly used: the wrist, as well as the ring finger.

2.8 Applications of Pulse Oximetry

Pulse oximetry is widely used in many clinical settings, including anesthesia, surgery, critical care, hypoxemia screening, exercise, and transport from operating room to the recovery room (7). Pulse oximeters for personal use are sold at several pharmacies and grocery stores. These are generally finger sensors. They will monitor oxygen saturation and heart rates. Other products, including the AquaPulse described in Section 2.13, have been designed for use in exercise. These are generally used as heart rate monitors to give the athlete feedback on the intensity of the workout.

2.9 Basic Assumptions of Pulse Oximetry

There are a few major assumptions that are made for pulse oximeters. Under these assumptions, they are very accurate (8). The first is that all hemoglobin present is either oxyhemoglobin or deoxyhemoglobin (8). This is not entirely accurate, as there are other substances in the hemoglobin, including carboxyhemoglobin and methemoglobin, as seen in Figure 2-1. However, these forms of hemoglobin do not contribute much to the signal. The second assumption is that there are no other absorbers between the light source and photodetector (8). This is obviously not true, as there is skin, bone, tissue, and venous blood that all contribute to the signal. The third, and possibly most important assumption, is that all the blood that pulsates is arterial blood (8). It is this assumption that is most violated by motion.

2.10 Limitations of Pulse Oximetry

While pulse oximetry is a widely used and relied upon technology, it does have several limitations. One limitation is that it makes the assumption that there are only two substances in hemoglobin, oxyhemoglobin and deoxyhemoglobin (2). It can be seen in Figure 2-1 that there are also other components of hemoglobin, including carboxyhemoglobin and methemoglobin. However, under most circumstances, these substances will not affect the reading (2). A second limitation is the photodetector used is susceptible to ambient light that can cause misreading. To correct for this, a form of shielding can be used or a measurement of the ambient light can be taken and then subtracted from the desired signal. Third, the pulsatile PPG signal is very small compared to the DC signal it is riding on (2). This can partially be corrected through the use of higher resolution A/D converters or brighter photodiodes (2). Low peripheral vascular perfusion, or a reduced level of blood in the limbs, can cause the signal produced to be too small to be reliably processed (7). These four limitations may cause some issues in the signal; however, the biggest problem that pulse oximeters are susceptible to is the addition of motion artifact to the signal. This will be covered in the next section, as it is the fundamental problem this study will explore, but could be caused from a variety of sources, including sensor displacement as a result of the motion. Below is a list of limitations that cause problems in pulse oximetry.

1. Assumption of only two substances absorbing and reflecting light
2. The photodetector is susceptible to ambient light
3. The pulsatile PPG signal is very small in comparison to the DC signal
4. Low peripheral vascular perfusion can cause the signal to be too small

5. Addition of motion artifact

2.11 Motion Artifact

Motion artifact is the largest contributor to poor signals in pulse oximetry. These poor signals may be caused by changes in arterial perfusion or normally non-pulsatile components, the B component of Figure 2-2, adding on to the pulsatile components, the A component of Figure 2-2. These components include venous blood, tissue fluids, fat, and muscle. Another cause may be sensor displacement.

Several studies have been performed to observe the effects of motion on pulse oximeters. One, performed by William Kist in 2002, tested two new pulse oximeters, the Nellcor N-395 and the Masimo ® SET (Signal-Extraction Technology) that claimed to eliminate motional artifacts (1). The results demonstrated a strong correlation between the two pulse oximeters on oxygen saturation and heart rate under both motion and non-motion conditions (1). However, the correlation between the two oximeters on heart rate was weaker under motion (1). It was discovered that the weaker correlation under motion was due to the Masimo system's inability to consistently determine heart rate during motion (1).

A paper authored by Michael Petterson discussed how motion artifact affects pulse oximetry accuracy (8). Petterson states that if motion is combined with low perfusion at the sensor, then the venous blood contributes even more to the pulsatile component and will cause even greater error in the signal (8). He cites a study performed by Tobin that

collected data on 35 patients determined a wide range of motions led to error but that most errors were generated by intense, aperiodic, random movements that last 30 seconds or less (8). The type of motion used in Tobin's study differs from the motion that will be necessary for this study. For the desired results of this research, periodic motion will also need to be effectively cancelled, and this motion would likely last significantly longer than 30 seconds and may coincide with the frequency of the heart rate. The periodicity of the interference is due to the general nature of motion that is performed while exercising; for example, the swinging of arms while running.

Another review, performed by Larry Mengelkoch and published in 1994, looked at 10 different studies that evaluated 24 different pulse oximeters that contained data collected during exercise (4). The review found that the degree of accuracy of the pulse oximeters was variable, even among the same models (4). He found that the studies reported mixed results of accuracy, with seven of the 10 studies having demonstrated that the pulse oximeters provide accurate results during exercise (4). Norton et al. found in 1992 that under exercise, there were relatively large underestimations of oxygen saturation and also cites several other studies that had findings that were in agreement with his (9).

Motion artifact has also been speculated to be caused by sensor displacement (5). Due to the rounded surface of skeletal bone, changes in the sensor position could cause changes in the backscattered light reaching the photodetector (5). An example of this is shown in Figure 2-5.

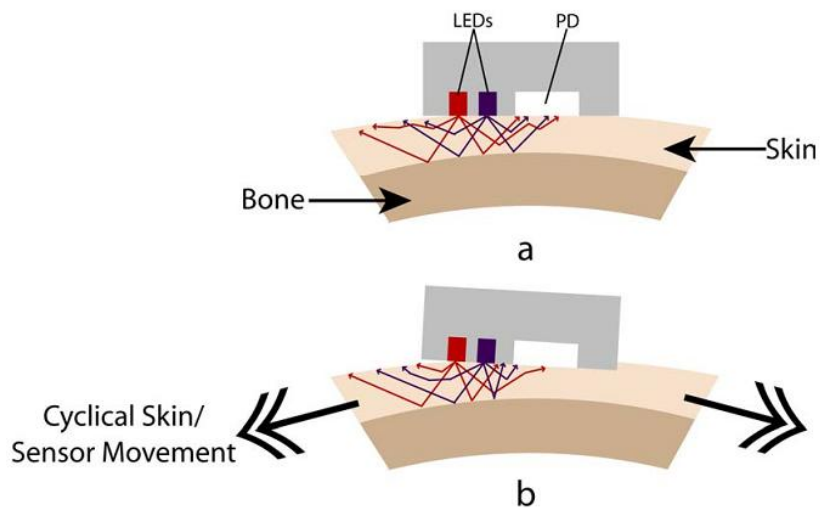


Figure 2-5: Sensor displacement altering backscattered light (5). (A) Typical light scattering before motion, (B) motion induced cyclical movement causes changes in sensor position, changing the backscattered light.

In work that was done using the system described in Section 2.12, it was found that motion greatly reduces the ability to extract a heart rate from the PPG signal. These results are in Section 5.

2.12 Current Device Features

The device used for much of this research was designed by Twisthink, LLC, based in Holland, MI. It consists of similar technology to off the shelf pulse oximeters, with one major difference: the use of only infrared LEDs. The goal of the device was to just monitor heart rate; therefore, a red LED is not necessary. The device utilizes the reflectance method described in Section 2.6, and was designed for use in a watch. There are four infrared LEDs and four photodiodes, with their power and bias voltages

controllable through software. The light produced by the IR LEDs will reflect off the blood that pumps through the arteries and will return to the photodiode, which will change its output voltage depending on the intensity of light received. The surrounding circuitry was standard operational amplifiers and filters currently used in pulse oximetry devices. With this design, the system was very susceptible to motional artifact, to the point where it could not extract a heart rate. These results will be discussed in Section 5.

2.13 Products Currently on the Market: Heart Rate Monitoring Watches

There are currently several different heart rate watches on the market. However, they generally require the use of a chest strap or some other form of accessory. Several companies advertise these watches to athletes, including Polar, Timex, and Garmin. They are also generally expensive, with Timex's Ironman watches being priced around \$200.00 and Garmin's being around \$400.00. An example of the chest strap these watches use is shown in Figure 2-6. Another watch that uses similar technology to the chest strap method, but applies it to the arm instead, is Impact Sports Technology's ePulse2, shown in Figure 2-7. These sensors must be in direct contact with your skin.

Other methods include those used by watches such as the Mio Classic that requires you to use two fingers pressed against the watch face to get the heart rate. This is a similar method to how most treadmills and larger exercise equipment get a heart rate. An example is shown in Figure 2-8.



Figure 2-6: Example of a heart rate monitoring watch using a chest strap



Figure 2-7: ePulse2 watch that uses chest strap technology on the arm



Figure 2-8: Example of heart rate monitoring watch using two fingers to extract a heart rate

A product that uses an infrared sensor to monitor capillary blood flow of the ear lobe to report the heart rate is the AquaPulse™, produced by FINIS, INC and released in June 2011. A picture of this, taken from the FINIS Inc. website, is shown in Figure 2-9. This is similar to the technology that will be used in this research, except the sensor will be at the wrist and ring finger instead of the ear.



Figure 2-9: AquaPulse Heart Rate Monitor using infrared sensor at the ear lobe

2.14 Current Techniques to Reduce Motion Artifact

This section will focus on studies that have used the techniques described to reduce motion artifact. A more in depth look at the specific filter types that are commonly used in biomedical signal processing can be found in Section 2.15.

2.14.1 Hardware

Analog filters with cutoff frequencies that are representative of potential heart rates should be used. A heart rate could be anywhere from 0 to 300 beats per minute, but most are between 50 and 150 beats per minute, or 0.83 to 2.5 Hz, unless there are extenuating circumstances. This will allow for the filtering of high and low frequency noise prior to the signals digitization.

2.14.2 Software

There are several techniques that are commonly used to “solve” the noise problem that pulse oximeters exhibit. Many of these techniques are applied with the hope of avoiding false alarms in hospitals (8). One technique is data averaging, in which the sampling time is increased so that the effect of motion is minimized (8). While this is a simple approach, it would not be applicable to motion that is period and extended, such as that of a runner. Another technique commonly used is data holding, which sees pulse qualified and only those fitting certain criteria are used in a calculation (8). Both of these techniques result in a loss of a significant amount of information (8).

At least two companies, Masimo and Philips, claim to have motion tolerant algorithms, however, these are highly proprietary (8). Masimo's SET technology "reads through motion" using several signal processing techniques including their proprietary Discrete Saturation Transform (8). It is comprised of a reference signal generator, an adaptive filter, and a peak picker (8). These are used to generate a power spectrum of the incoming signal (8). Philip's FAST SpO₂ (Fourier Artifact Suppression Technology) depends on a frequency based algorithm that first identifies the frequency components of the incoming signal that is at the pulse rate for both the red and infrared wavelengths (8). It is this component that is used to calculate oxygen saturation (8).

Another technique implemented by Hayes proposes that, through the use of a signal processing method based upon inversion of a physical artifact model, the effects of motion can be greatly diminished (10). He states that many of the approaches used to reduce corruption are based on signal processing techniques that make assumptions about the expected signals, usually frequency related, statistical properties of the signal, or the degree of correlation with the signal and those signals from another transducer (10). Hayes goes on to state that he believes all of these signal processing methods suffer from the generality of the assumption that the artifact presents itself as an additional signal component that does not affect the physiological measurement (10). He proposes that instead of using the linear assumptions that most methodologies employ, there should be a shift to a nonlinear artifact reduction method (10). This system will change the calibration technique for oxygen saturation (10). A description of this technique was published by the same author a few years prior to the study mentioned above (11). It is

argued that the linear model used to attempt to cancel motion artifact is inaccurate for certain motions, especially those that alter the distance between the source and detector (11). In this publication, it is demonstrated that by altering the normally linear model used for PPG signal, a nonlinear response characteristic can be used to renormalize the signal so that it can be easily interpreted (11). Through the use of this new model, the motion artifact model is also changed into an additive form that is more easily removed (11).

Another study, performed by Meltem Izzetoglu, proposes the cancellation of motion artifact through the use of discrete Kalman filtering (12). It was found that the performance of the Kalman filter achieved a better signal to noise ratio than the adaptive filtering technique used by Izzetoglu in a previous study and results were comparable to Wiener filtering (12). Izzetoglu studied the effects of using Wiener filtering using the same data used in the Kalman filtering study (13). For the adaptive filter, accelerometer data were used to successfully suppress motion artifact except for the first data points in which the filter could not adapt itself because of a lack of information on the data (13). Wiener filtering on the same data set yielded better signal to noise ratios (13). However, one major problem using the Wiener filter is that it worked offline, meaning that the whole data set had to be collected prior to filtering (13).

In a 2005 study performed by Yong-sheng Yan, it was proposed that the use of a smoothed pseudo Wigner-Ville distribution could be used to reduce motion artifact on wearable pulse oximeters (14). The difference between this method and a normal

Wigner-Ville distribution is that it accounts for “cross-term interference” by incorporating two windowing functions (14). When it was compared with a weighted moving average approach and a fast Fourier Transform approach, the Wigner-Ville distribution approach showed a significant improvement in the pulse rate estimation when the subjects were in motion (14). He determined that the Wigner-Ville distribution had a much higher time-frequency resolution and can therefore be used more easily than other techniques to obtain a cardiac frequency, or heart rate (14). In 2008, Yan described a minimum correlation discrete saturation transform (MCDST) that showed to be more accurate and robust than the Masimo discrete saturation transform (15). This technique was designed for a wearable pulse oximeter and makes the claim that it is more computationally efficient because it uses linear algebra instead of adaptive filtering (15). This method employed a new ratio of ratios for both arterial and venous blood oxygen saturation (15). The algorithm first collects both red and infrared signals and calculates the normalized pulsatile signals of each, calculated the constrained relationship between the new ratios, synthesized the reference pulsatile signal and motion artifact, and then obtained the MCDST spectrum and identified local minimums in the spectrum to determine the values of oxygen saturation (15).

In 2005, Peter Gibbs presented a technique for reducing motion artifact in wearable biosensors by using accelerometers for active noise cancellation (16). Gibbs paired an accelerometer with a finger ring PPG sensor and used an adaptive filter under two different assumptions: the motion artifact was additive and the motion artifact was multiplicative (16). A large correlation between the accelerometer signal and the PPG

signal was found (16). Data was sent through a recursive least squares (RLS) adaptive filter algorithm and the corrupted PPG signal was successfully reconstructed for both the additive and multiplicative models using one axis of the accelerometer (16). He concluded that active noise cancellation using accelerometers is an effective method to produce motion tolerant wearable sensors (16). This study will attempt to confirm Gibbs's conclusion.

2.15 Filtering Techniques

This section will cover the most commonly used filtering techniques used in pulse oximetry.

2.15.1 Adaptive Filtering

Adaptive filters have been used repeatedly in the efforts of noise cancellation in electrocardiograms (ECG) and electroencephalograms (EEG), among many other biomedical signals (13). There are several different algorithms, such as least mean square (LMS), normalized least mean square (NLMS), frequency domain and sub-band adaptive filters and recursive least squares (RLS) filters (13). Due to its simplicity, LMS adaptive filters became the standard adaptive filter used (12). This filter has two inputs, the primary input, which consists of the desired signal plus the noise, and the reference input, which is a correlated signal with the noise present in the primary input (13). The reference signal is obtained from a separate measurement (13). The filter coefficients are updated at each time point by using the two inputs to estimate the signal (13). The output is an estimate of the noise in the primary signal, meaning that the original signal is the

primary input minus the output of the filter (13). Figure 2-10 shows the block diagram for an adaptive filter.

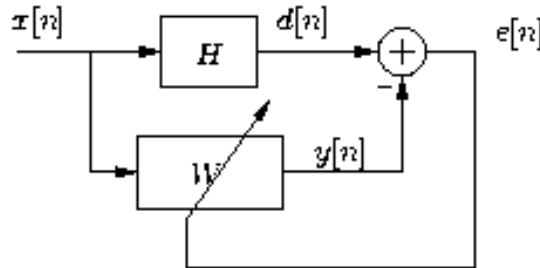


Figure 2-10: Adaptive Filter Block Diagram (17)

2.15.2 Wiener Filtering

The basic concept of a Wiener filter is to minimize the difference between the filtered output and some desired output (18). It does this by minimizing the mean-square error (MSE) with the goal of filtering out noise that has corrupted a signal through the use of the least-mean-square approach, which adjusts the filter coefficients to reduce the square of the difference between the desired output and the filtered output (18). The input signal contains both the signal and the noise that is needed to be cancelled (18). This type of filtering operates under the assumption that the signal and noise are stationary linear processes with a known spectral content (13). A stationary system is one that has a probability distribution that does not change when the process is shifted in time or space. It is this that separates it from being an adaptive filter. One large issue with this type of filtering is that it cannot be done in not real-time, meaning that the whole data set must be collected prior to filtering it (13). Figure 2-11 shows the block diagram for a Wiener filter.

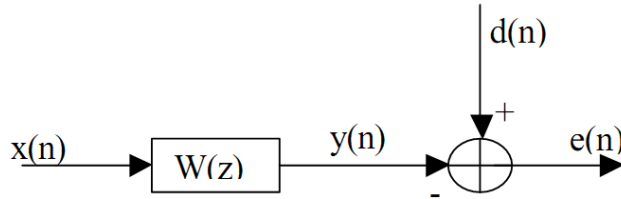


Figure 2-11: Wiener Filter Block Diagram

2.15.3 Kalman Filtering

Kalman filtering uses a state space representation and least squares estimation methods for the recursive estimation of signals of interest that are buried in noise (12). This algorithm has been widely used in navigation and guidance systems, radar tracking, sonar ranging and satellite orbit determination (12). Kalman filtering produces estimates of the true values of a corrupted measurement and their associated calculated values by predicting a value, estimating the uncertainty of the predicted value, and computed a weighted average of the predicted value, and computing a measured value. The recursive nature of the filter makes it very appealing compared to other techniques because the practical implementations are much more feasible (12). However, the practical implementations are still not as feasible as an LMS algorithm. Figure 2-12 shows the block diagram for a Kalman filter.

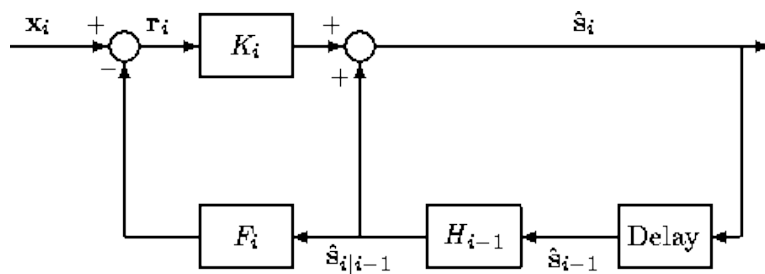


Figure 2-12: Kalman Filter Block Diagram

2.15.4 Wigner-Ville Distribution

The Wigner-Ville distribution of a signal is calculated using the instantaneous autocorrelation function and the distribution is invariant to shifts in time and frequency (18). To obtain the distribution, the Fourier transform of the instantaneous autocorrelation function is taken, but only along the lag dimension. The output of this distribution is a function of both time and frequency (18).

2.15.5 Wavelet Transform

The Wavelet Transform (WT) provides a good representation of the signal with both good frequency and time resolutions (19). The WT can be used to describe properties of a waveform that change over time (19). The transform is a signal decomposition from a set of basis functions obtained by dilations, contracts and shifts of a unique function, which is the wavelet prototype (19). The WT basis functions have a frequency dependent width that gives it the ability to zoom in on local phenomena (19). Such zooming could be advantageous to filtering motion artifact that does not present itself over an extended period of time. The discrete wavelet transform uses groups of filters to divide the signal in to various spectral components (18). These filter banks consist of varying responses, such as low and high pass, that divide the signal into different components that can later be added back to reconstruct the original signal (18). This technique was used by Balasubramaniam as a noise cancellation algorithm on an ECG signal and was used for detection of heart rate, amplitude and timings of the ECG (20). By using the Daubechies DB4 wavelet, a noisy ECG signal was filtered to contain significantly less noise (20). Figure 2-13 shows the block diagram for a wavelet transform.

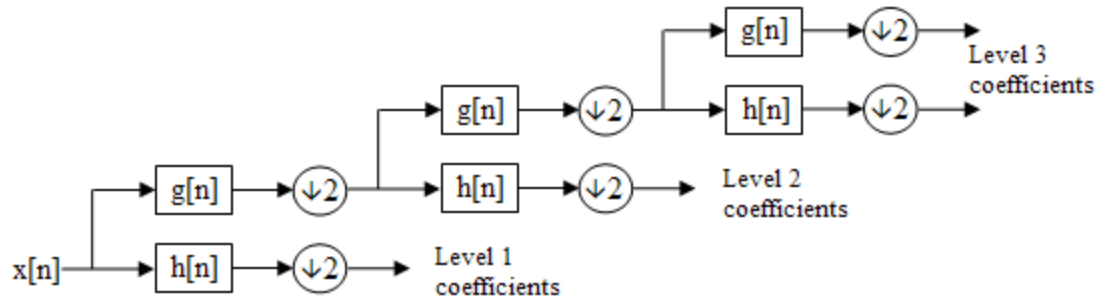


Figure 2-13: Wavelet Transform Block Diagram

2.15.6 Weighted Moving Average

This method is useful for evaluating signals that have valleys but no sharp peaks in its frequency content (18). This model has only the feed-forward filter coefficients and has the same defining equation as an FIR filter (18).

3 SPECIFIC AIMS

Motion artifacts strongly corrupt heart rate measurements in current pulse oximetry systems. In many, almost any motion will greatly diminish the system's ability to extract a reliable heart rate. The artifact is most likely present due to normally non-pulsatile components of the body, such as venous blood and tissue fluid, which become pulsatile during motion. Displacement of the sensor is also a major cause of the artifact. Through the use of hardware, software, and signal processing techniques, a wearable heart rate monitor that is less susceptible to motional artifact will be investigated. The final goal will be to attempt to design a device that can reliably extract the subject's heart rate despite the presence some level of motion artifact. The following steps will be followed in the attempt to reach the goal:

1. Collect data using the pulse oximetry device described in Section 2.12.
 - a. Include data from 3-4 subjects
 - b. Collected data for a resting signal
 - c. Collecte data for aperiodic motion: such data will consist of motion that is seemingly random and not in a cyclical form.
 - d. Collecte data for periodic motion: Due to the desire to be able to use this device during exercise, data consisting periodic motion, such as the swinging of arms while running, needs to be collected.
2. The data collected in step 1 will then be filtered. The first test filter is an LMS adaptive filter with the two input signals being the PPG signal with any additional noise and signals obtained from using an accelerometer. The output of the filter

should be a reconstruction a clean heart rate signal. If the noise is not significantly cancelled, other filter techniques, including RLS adaptive filters, Kalman and Wigner-Ville, may be explored.

3. Once the data is filtered, analysis will be performed to determine the effectiveness of the filter. Such analysis will consist of determining the signal to noise ratio and the extent to which the filtering method improves it. If it is not sufficient, step 2 will be repeated with a new filtering technique.

4 METHODS

4.1 Integrated Pulse Oximeter and Accelerometer Wrist and Finger Sensor

The device described in Section 2.12 was used for much of this research was designed by Twistthink, LLC, based in Holland, MI. With this design, the system was very susceptible to motional artifact, to the point where it could not extract a heart rate with only small amounts of unidirectional motion. The device was then modified to include an accelerometer and two red LEDs. The accelerometer detects the motion that corrupts the heart rate measurement. Figure 4-1 shows the new device. The flexible circuit board connected to the device wraps around the wrist to illuminate the arteries travelling through the arm. The flexible circuit board was also wrapped around a finger like a ring for more testing.

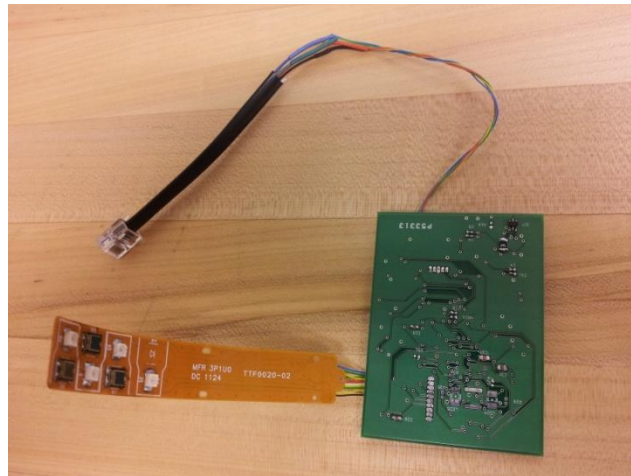


Figure 4-1: Prototype with integrated accelerometer and heart rate detector

4.2 Data Gathering

Data were gathered through the use of two devices, one for a reference signal and one for the corrupted signal, and a computer based user interface. The two devices were each placed on either wrist of the subject. Data were also gathered from ring fingers as a comparison to the wrist sensor. One arm was kept still so that it could be used as a

reference while the other was allowed to move with multiple degrees of freedom during the experiment. The data was acquired through a UART to USB data line. Figure 4-2 shows results from one experiment. The bottom signal is z-axis of the accelerometer, as it was the main axis of motion and the top signal is the corrupted heart rate signal. In the figure, the y-axes are the representative amplitude values for the signals: voltage for the heart rate and acceleration (G's) for the accelerometer. Both the signals were 10 bits, meaning that they had values from 0 to 1023. For the heart rate, these values correlated to a voltage between 0 and 3 volts. The accelerometer signal represented acceleration between -4G and +4G. The data were read in by a program written in National Instruments LabWindows CVI and functioned as the user interface, shown in Figure 4-3. It allows for changing of the LED and photodiode selection, photodiode bias, and LED power. Data sample rate is also adjustable using this interface. To assist display, the data were low-pass filtered to remove high frequency noise inherent in the accelerometer and heart rate signals. Finally, data were written to text files for later analysis.

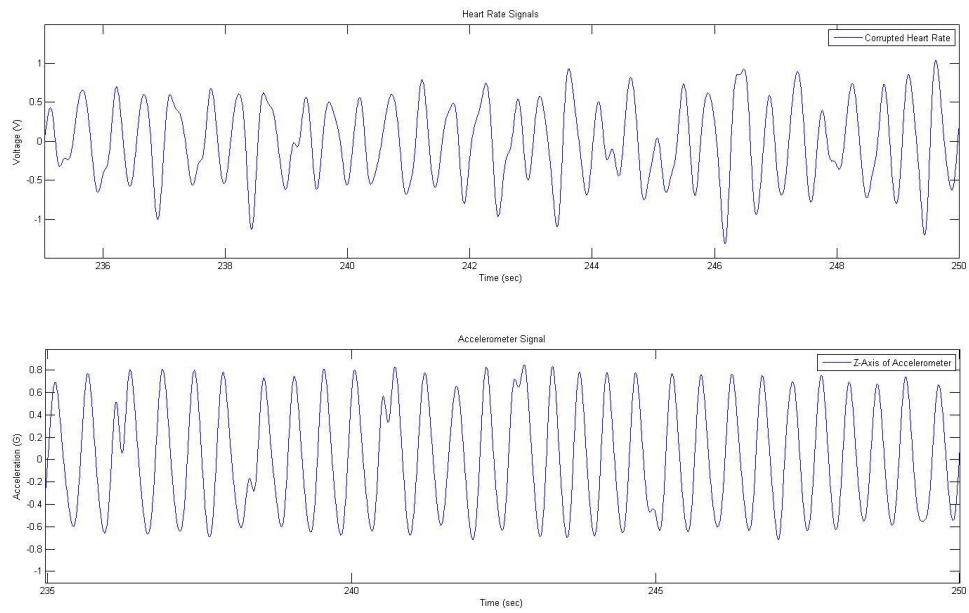


Figure 4-2: Results from motion: The top plot is the corrupted heart rate signal and the bottom plot is the z-axis of the accelerometer

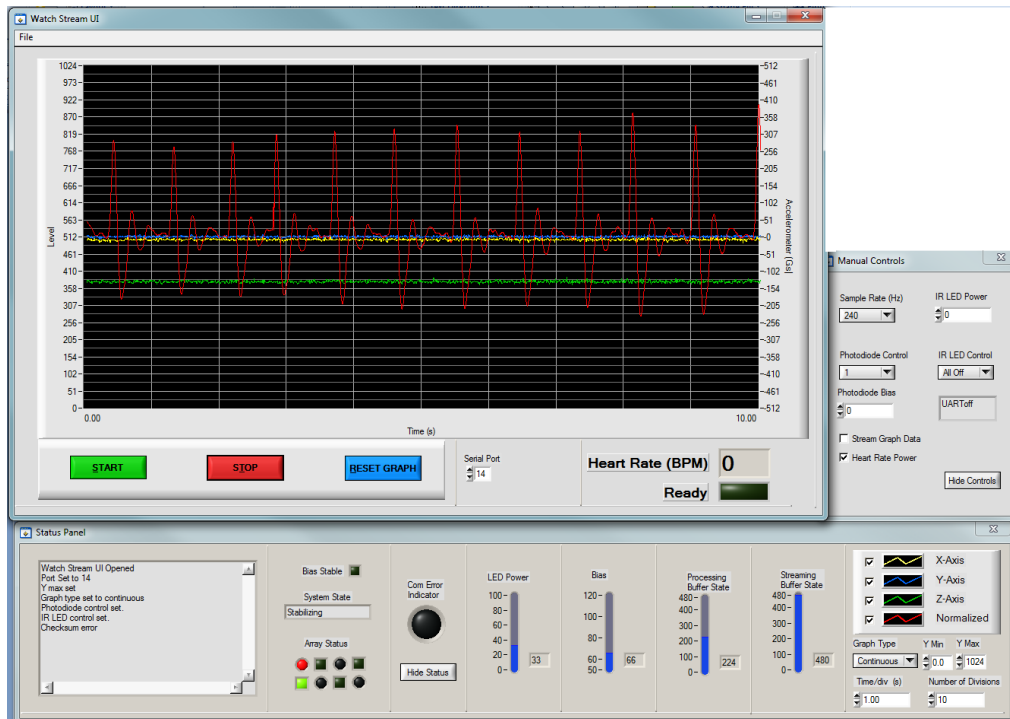


Figure 4-3: Screen capture of the user interface used to collect the signals

4.3 Additive Distortion Model

The pulse measurement is distorted by motion and any sensor attempting to measure that signal will be measuring a combination of the desired signal and an interference signal. The simplest way to model this situation is to assume that the two signals are additive (16). Figure 4-4 shows the principle of this in a block diagram. The true, uncorrupted signal is labeled as h_0 , the measured signal is labeled as h , and the distorted signal as w . The body motion is detected by an accelerometer, a , and an adaptive filter will estimate the distorted signal, \hat{w} . The estimated distorted signal is then subtracted from the measured signal, leaving an estimate of the pulse signal as the filter output. There is an inherent assumption of linearity in an additive distortion model: the measured interference signal is linearly related to the corrupted heart rate signal, allowing it to be derived through an iterative algorithm. Assumptions for this model are discussed further in Section 4.5.3.

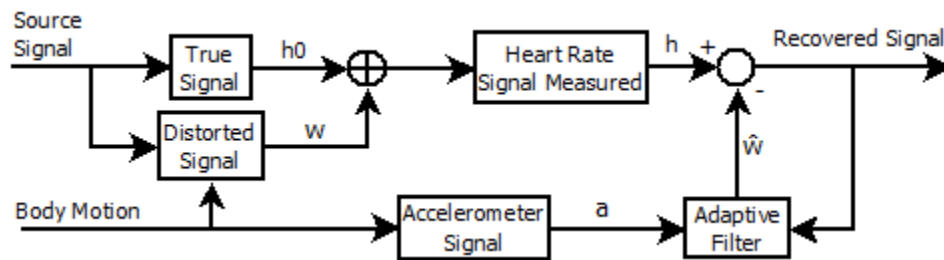


Figure 4-4: Block diagram of the additive distortion model adaptive filter

4.4 Correlation Analysis

Once the data were collected, the next step was to determine if there was actually a correlation between the motion artifact in the heart rate signal and the accelerometer signal. It is known that bio rhythms tend to align and become correlated, especially a whole-body repeated motion, such as a swinging arm in a jogger (21). In particular,

human strides, including hand motion, synchronize with the heart pulsation when the frequencies of each signal are near each other, which is a common case while walking or jogging (21). This alignment could cause a problem in which the heart rate signal is filtered out with the interference signal.

Referring back to Figure 4-2, it is clear that the corrupted heart rate signal differs greatly from what a normal heart rate looks like. The two signals have first peaks that do not occur at exactly the same time. This non-alignment implies that there is some form of delay that occurs between the acceleration and its effect on the heart rate signal. This delay is vital to know so that the inputs to the adaptive filter can be modified prior to filtering, allowing the filter to converge on a solution quicker. To determine the delay, the correlation of these signals is calculated. The corrupted heart rate signal is h and the correct heart rate signal is h_0 . Using the additive distortion model, the distortion signal can be modeled as:

$$\hat{w} = h - h_0$$

The above model assumes that the reference heart rate signal measured is approximately equal to the correct heart rate signal from the moving arm had it been stationary.

However, movement of the one arm will affect the blood flow through the rest of the body, including the stationary, reference arm. To quantify the delay, a normalized correlation between the accelerometer signal and the distorted heart rate signal was calculated using the equation below, where μ , σ are the mean and standard deviation of each of the signals, and d is the time delay. In the equation, N is the length of each signal and m is maximum delay length.

$$Cor(\hat{w}, a; d) = \frac{1}{N - m - 1} \frac{\sum_{i=0}^{N-m-1} (\hat{w}_{i+d} - \mu_{\hat{w}})(a_i - \mu_a)}{\sigma_{\hat{w}}\sigma_a} \quad (1)$$

The model of Figure 4-4 has limitations in practice. The peaks of the heart rates retrieved from both arms occur at different times, making it difficult to subtract one from the other to rid the corrupted signal of the pulsing of the heart rate. This could be due to the sensors not being exactly the same or slight differences in the physiology and anatomy of each wrist or finger. Also, local vascular control has the ability to regulate the artery blood flow differently in each finger (21). The differences can be seen in Figure 4-5. These two signals were acquired at the same time from sensors with the exact same design. It is evident that the signals have different amplitudes but there is also a time delay between the two that is inconsistent. When performing the subtraction at the point of highest correlation between the two signals, the resulting signal still has significant peaks because of the inconsistent offset, as seen in Figure 4-6. Given this evidence, it was decided to just use the corrupted heart rate signal in the correlation analysis, even though it has the pulsatile component from the heart beating still present.

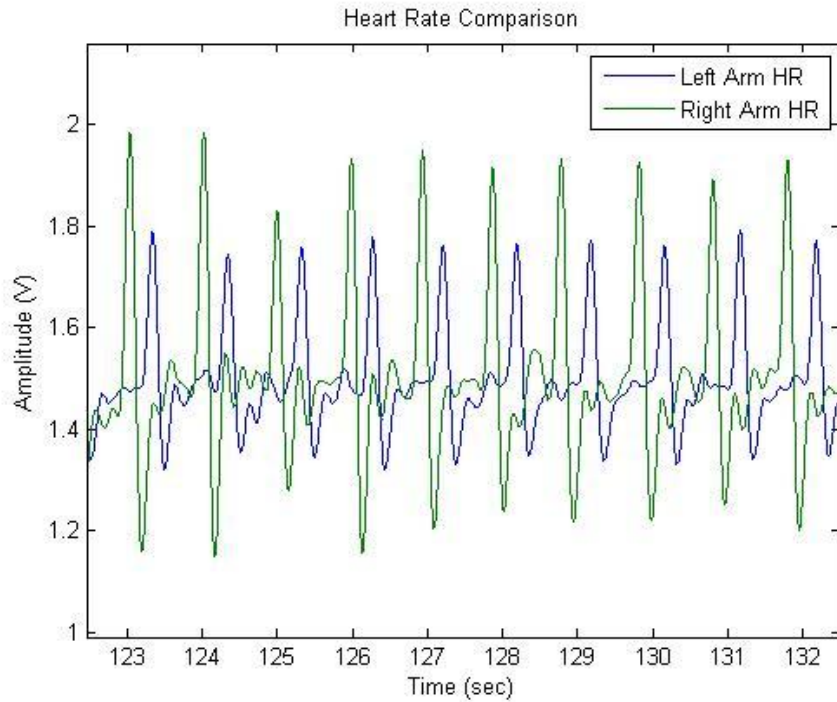


Figure 4-5: Comparison of heart rate signals from opposite arms

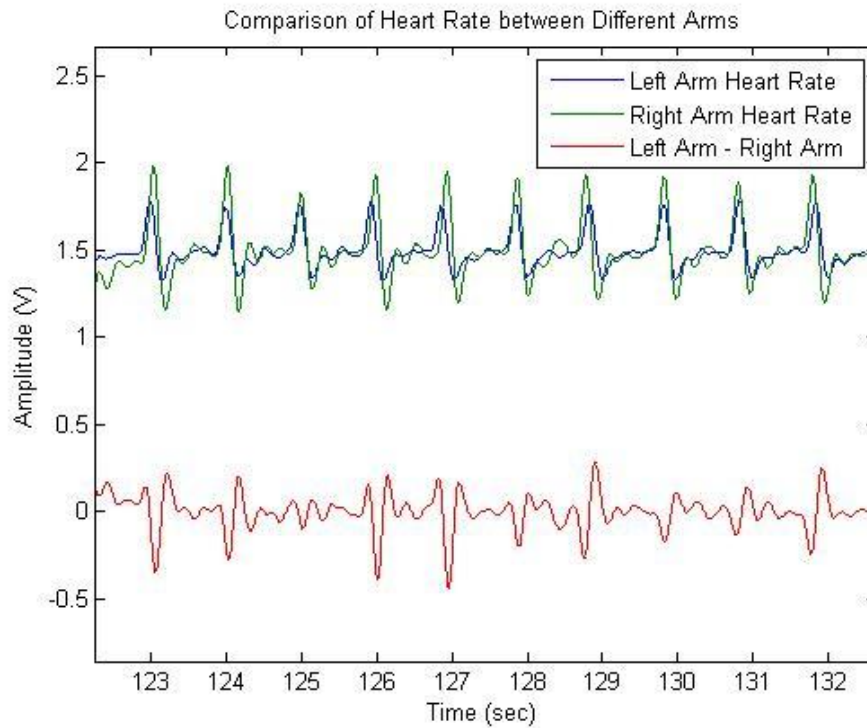


Figure 4-6: Subtraction of heart rates from the left and right arm

Due to the failure of the additive distortion model, a custom algorithm was developed which utilized five second windows of data. The correlation of each window was then calculated. A step size of 1 second was used, meaning that the first section of data was 0 through 5 seconds; the second was 1 through 6 seconds and so on. This was done for the whole data set and for every data set. This algorithm discovered the five second window in the data set that had the highest correlation between the corrupted heart rate signal and the main axis of motion on the accelerometer. The time lag of the maximum correlation reveals the ideal time delay between the heart rate signal and the accelerometer signal. The window with the highest correlation was then adaptively filtered. It is important to note that each signal was shifted to have a mean of zero for the time period.

4.5 Adaptive Filter Model

Based on the correlation analysis, an adaptive filter model was created that would predict the distortion of the heart rate signal in response to the acceleration. The window with the highest correlation was utilized and the accelerometer signal was delayed to the ideal time to match the heart rate signal. The resulting model is a Finite Impulse Response (FIR) filter with the specific time window having a high correlation with the acceleration signal. Two types of FIR filters were used: Least Mean Squares (LMS) adaptive filter and Recursive Least Squares (RLS) adaptive filters. Both of these filter types attempt to minimize error signals and were chosen because they are commonly used in biomedical signal processing. An LMS algorithm would be simpler to implement in a real time system but an RLS algorithm will converge on a solution faster. The filter was constructed in MATLAB and source code for the algorithms is given in Appendix A.

4.5.1 Least Mean Squares Adaptive Filter

The goal of an LMS adaptive filter is to minimize the least mean square of the error signal, which is the difference between the desired signal and the actual signal. This filter has two inputs, the primary input, which consists of the desired signal plus the noise, and the reference input, which is a correlated signal with the noise present in the primary input (13). The reference signal is obtained from a separate measurement (13). The filter coefficients are updated at each time point by using the two inputs to estimate the signal (13). This output is an estimate of the noise in the primary signal, meaning that the original signal is the primary input minus the output of the filter (13). Referring back to Figure 4-4, a is the accelerometer signal and is the reference input; h is the measured signal from the heart rate sensor and consists of the heart rate signal and the interference signal; \hat{w} is the filter's estimation of the interference signal; and the recovered signal is the filter's error signal.

Two parameters had to be set for the filter: the length, or number of coefficients or taps of the filter, and the step size. The step size must be chosen carefully. If it is too small, the time the filter takes to converge on the correct coefficients increases. A step size that is too large can cause the filter to become unstable and not converge on the correct coefficients. Due to the relatively short window, a higher step size must be chosen.

4.5.2 Recursive Least Squares Adaptive Filter

The goal of an RLS adaptive filter is to minimize the sum of error squares. In an RLS filter, the signals are assumed to be deterministic, meaning that there is no randomness and it likely has some periodicity to it. An LMS filter assumes the signals are stochastic,

or random. Like the LMS filter, two parameters need to be set: the length of the filter, which will determine the number of coefficients and the forgetting factor of the filter. This will determine how many previous error calculations are held in memory. The LMS filter only looks at the current error value. For this study, the forgetting factor was left at 1, meaning the filter had infinite memory of the previous error values. The length of the filter was chosen to be the same as the LMS filter to maintain consistency across the two techniques.

4.5.3 Model Assumptions

There are assumptions that must be made for the filter model. The corruption model presented in Section 4.3 implicitly makes two assumptions about the corruption in the heart rate signal.

1. Linearity: motion in the heart rate artifact responds linearly to the motion inputs
2. Additivity: the motion artifact adds to the heart rate induced light intensity to create the corrupted signal that is measured

Linearity is desired so the filter can create an accurate model. If the system is not linear, the filter will be unable to model it. However, in the system, which is governed by the Beer-Lambert law, the measured light intensity actually varies exponentially with the distance it travels through the absorbing material. It is also unknown exactly how the motion affects changes in measured blood volume (21).

The additive characteristic is important because if the motion does not present itself by adding to the heart rate signal, the model will not accurately model the system. For

instance, Gibbs suggests that it could have a multiplicative or logarithmic effect on the measurement (16). It is also unknown how the arterial walls and the surrounding tissues respond to the movement or how the blood is redistributed (21). How these effects are superimposed on the actual heart rate signal is thus unknown (21). If either of these assumptions does not hold true, the model will likely fail.

4.5.4 Filter Resolution

As mentioned previously, the sampling rate for both the accelerometer and the heart rate was 240 Hz. The average heart rate will be between 0 and 5 Hz at a maximum, which would correlate to 0 and 300 beats per minute. The motion of the arm will be in this same range. With these two frequencies considered, the Nyquist Frequency would be 10 Hz. The 240 Hz sampling rate is 24 times higher and is sufficient for this system. Dividing the sampling rate by the length of the filter will give a filter resolution of 24 Hz per coefficient. This means that each coefficient will account for 0.04 seconds.

A normal resting heart rate will be approximately 1 Hz. With the system used, 1 Hz cannot be resolved. For a filter to be able to resolve this, it must have 100 taps. Increasing the number of taps to 100, which is 10 times the number used, would greatly increase the time the filter takes to converge. It would not be able to start calculating the output until 0.4 seconds of data were processed. This is 8% of the data in the five second window used.

5 RESULTS

5.1 Data Collection Analysis

Data were collected from two different places. The first was the wrist and the data was very easily corrupted from motion along any axis. Differing from the wrist, data collected from the ring finger was corrupted from mainly one axis of motion: the axis that is parallel to the digital artery in the finger. The vascular anatomy of the arm and hand is shown in Figure 5-1.

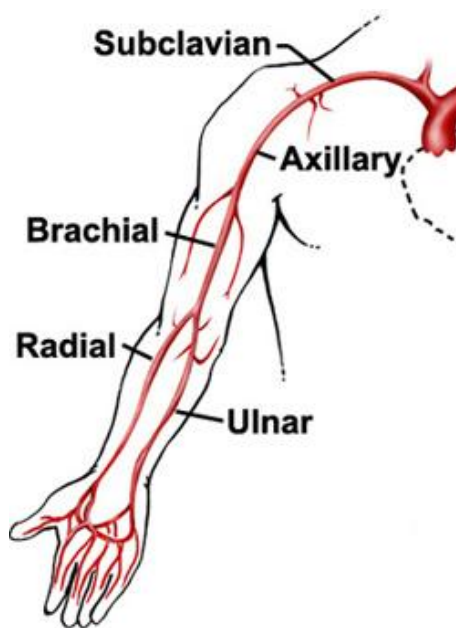


Figure 5-1: Vascular anatomy of the arm and hand

At the wrist, motion on any axis corrupted the signal. This could be due to a more complicated anatomy of the region, which contains more bone, muscle and tissue than the finger does. Figure 5-2 through Figure 5-4 show how, in the same orientation, the sensor can be corrupted by motion in any direction. This is in sharp contrast to the sensor at the finger, which can be subjected to a significant amount of motion in two axes. However, very little motion in the axis that is parallel with the digital artery will corrupt the heart rate signal. This is shown in Figure 5-5 and Figure 5-6.

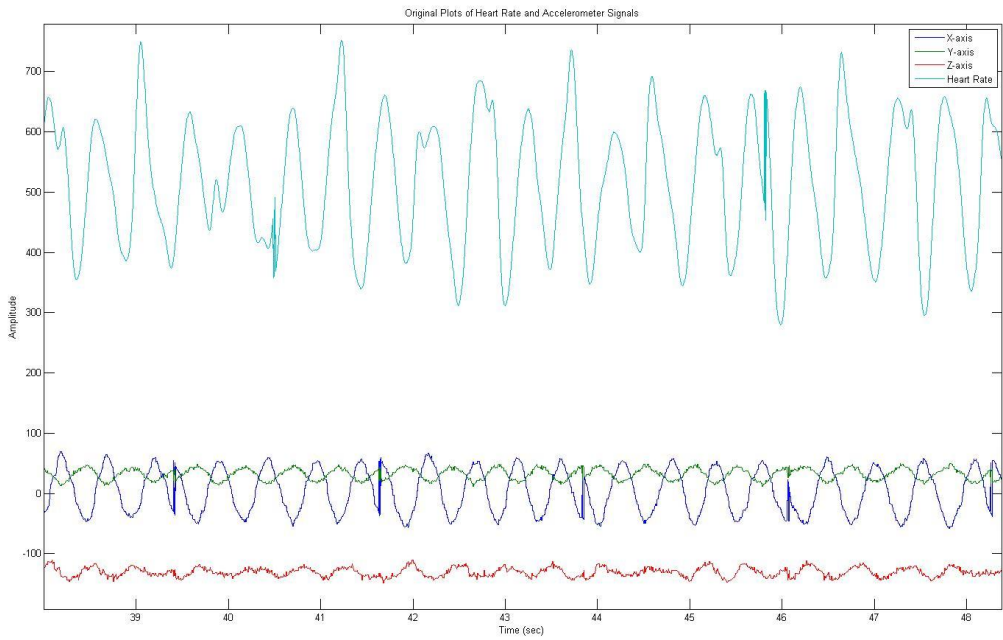


Figure 5-2: Motion corruption on the wrist in the x-axis

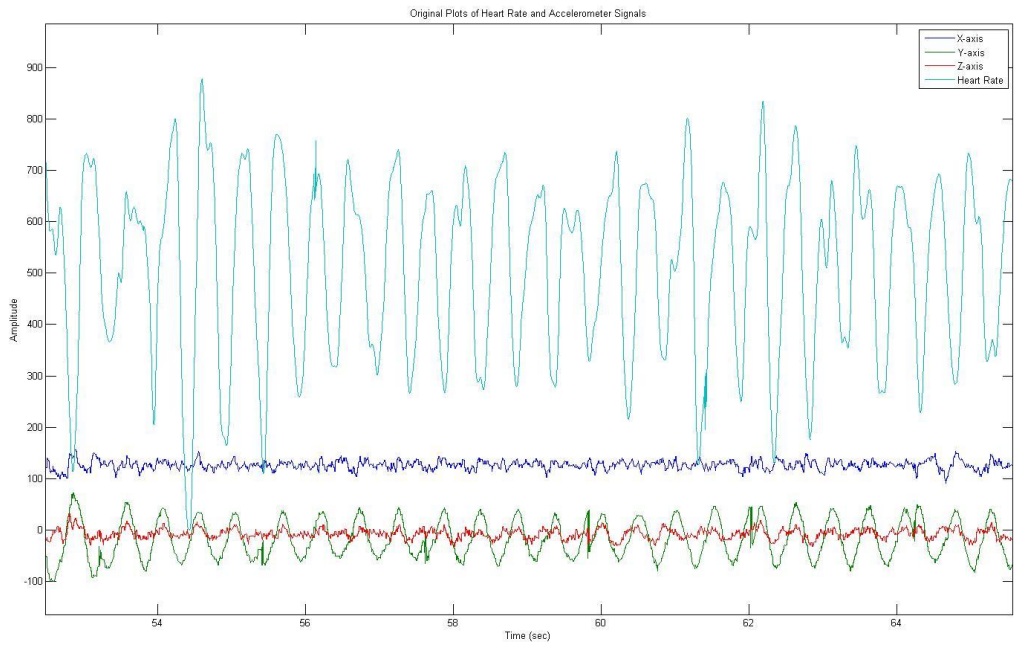


Figure 5-3: Motion corruption at the wrist on the y-axis

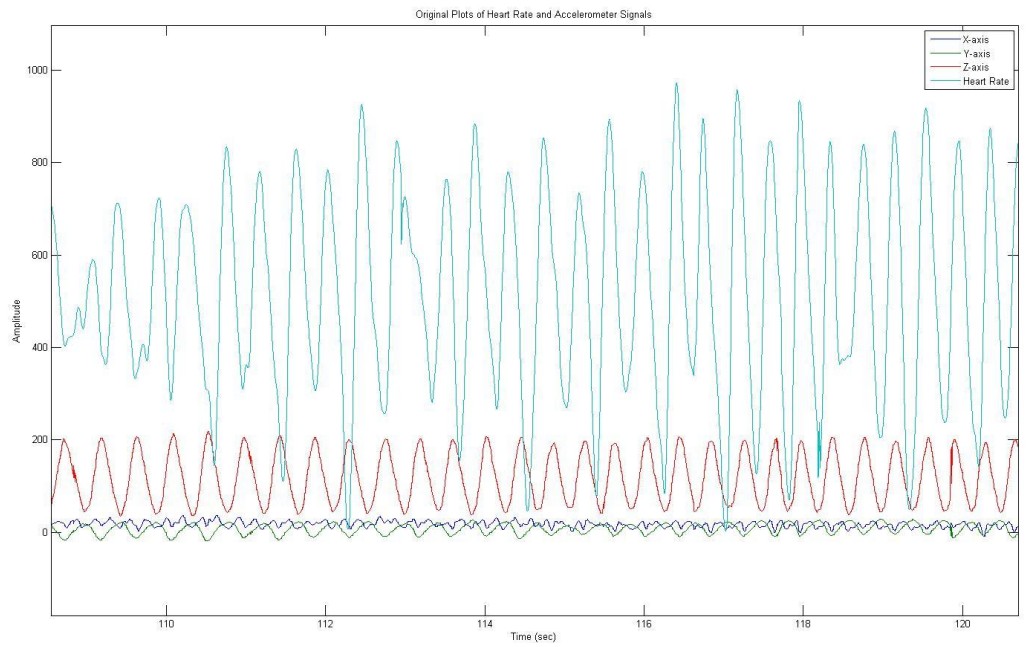


Figure 5-4: Motion corruption on the wrist on the z-axis

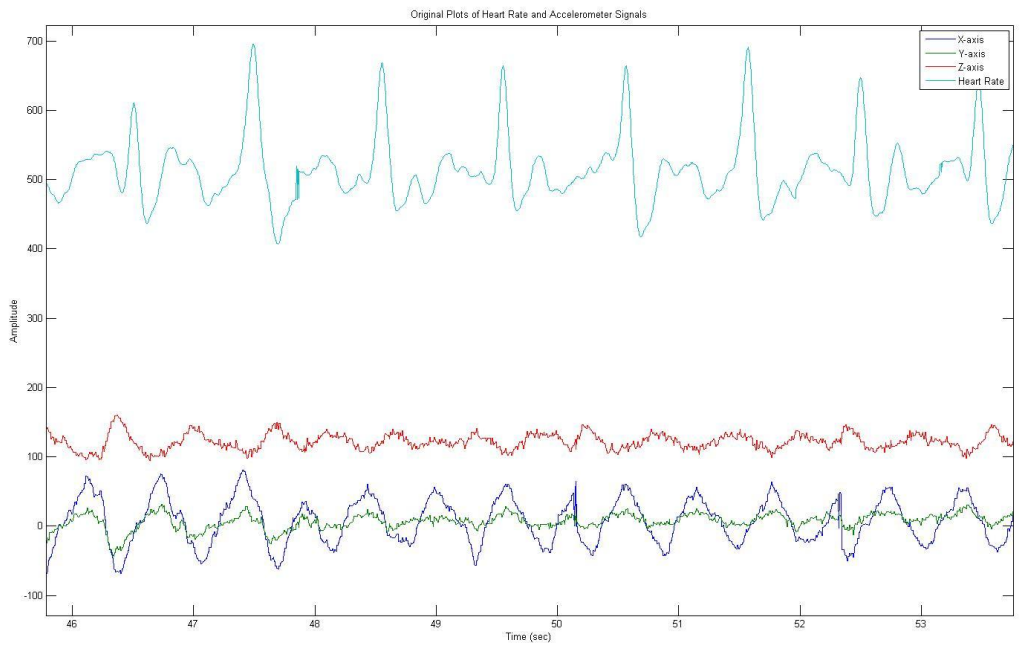


Figure 5-5: A lack of motion corruption at the ring finger despite significant motion on the x-axis

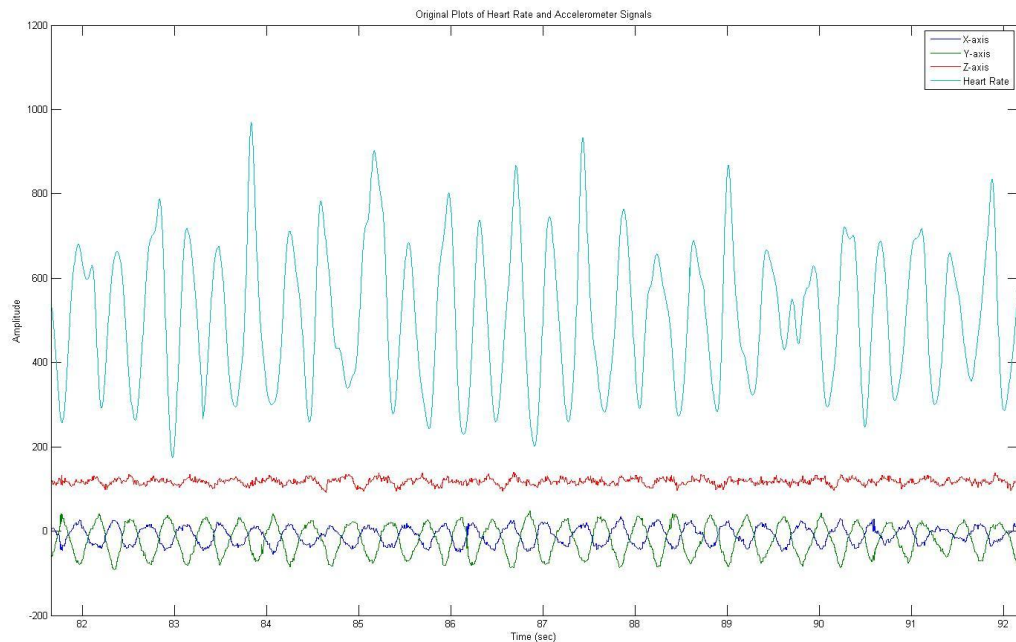


Figure 5-6: Motion corruption in the axis parallel to the digital artery at the ring finger

5.2 Correlation Analysis

The maximum correlation window for each data set had a varied result and a varied lag time. There were 18 data sets collected at the wrist and 11 at the finger. Each data set went through the correlation analysis. The five second window with the maximum correlation was found and that maximum, along with its lag time, were recorded. The sets were then separated by the type of motion that was performed in each set: longitudinal, motion in the parallel axis of the arteries, and side to side, or motion perpendicular to the axis with the arteries. The correlation for the whole data set was calculated, although it has been determined that this is largely not useful, as the correlation is very low and the lag time is too long. For this reason, the windowing system described in Section 4.4 was implemented. The mean correlations for each type of motion, along with the mean lag times, were calculated. This data is shown in Table 5-1 and Table 5-2.

Table 5-1: Correlation data for the wrist data sets: Averages (include standard errors)

	Full	Standard Deviation	Lag Time (sec)	Standard Deviation	Windowed Signal Correlation	Standard Deviation	Lag Time (sec)	Standard Deviation	Sample Size
Longitudinal	0.1555	0.0506	14.8862	13.3996	0.6312	0.0657	0.4014	0.3623	9
Side to Side	0.1785	0.0602	16.9792	11.4816	0.7514	0.0957	0.2292	0.5553	7

Table 5-2: Correlation data for the ring finger data sets: Averages

	Full	Standard Deviation	Lag Time (sec)	Standard Deviation	Windowed Signal Correlation	Standard Deviation	Lag Time (sec)	Standard Deviation	Sample Size
Longitudinal	0.1944	0.0804	8.1021	7.0023	0.7753	0.0657	0.1375	0.0887	6
Side to Side	0.1169	0.0193	8.5603	7.1964	0.6570	0.1086	0.3125	0.4501	5

Figure 5-7 shows the output of a window that has a maximum correlation of 0.7215 at 0.1625 seconds. This implies that the effects of the acceleration do not appear in the heart rate signal until 0.1625 seconds after the motion has taken place. As seen in Table 5-1 and Table 5-2, this lag time is representative of the ring finger data, which had an average lag time of 0.1375 seconds. A t-test was performed and the mean correlations for the wrist and the ring finger showed no statistical difference, with a p-value of 0.354. One interesting point is that the average lag time for the wrist in the direction of the arteries is actually higher than the side to side motion artifact. This is the opposite of the finger, where it is almost 3 times shorter in the longitudinal motion. The same holds true for the windowed signal correlation. The longitudinal direction has a higher correlation than the side to side motion at the ring finger, while it is the opposite for the wrist.

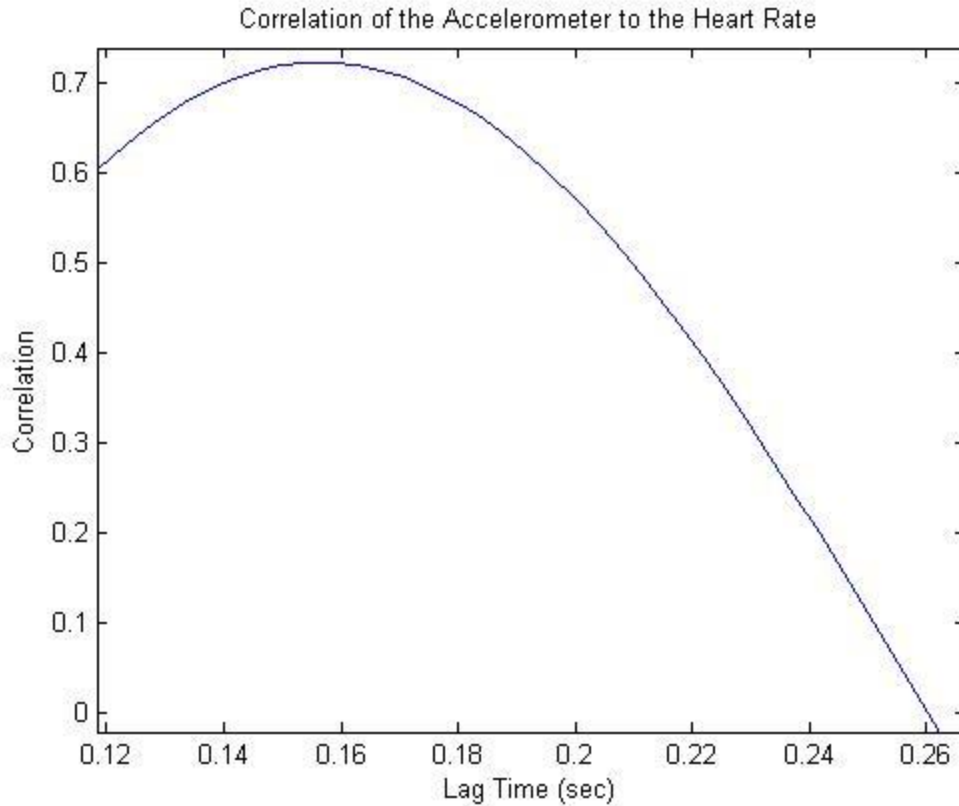


Figure 5-7: Example of a correlation output

5.3 Adaptive Filter Results

The LMS and RLS filters described in Section 4.5 were implemented on each window set that contained the maximum correlation. Both filters yielded similar results on each data set. Through properly choosing the filter characteristics, the filters successfully remove large portions of the motion artifact. However, they generally did not leave usable heart rate signals.

5.3.1 Wrist Sensor Filter Results

Below are the plots of the data sets from the wrist that had the highest correlation and resulting LMS and RLS filter results. These are representative of how the filters functioned for the majority of data sets. Figure 5-8 shows the five second window that

will be processed by the LMS and RLS filters. These signals were acquired from the wrist sensor. It can easily be seen that there is a high correlation between the heart rate sensor output and accelerometer signal. This window was at the end of a segment of motion and was chosen because of the high correlation between the heart rate and accelerometer signals.

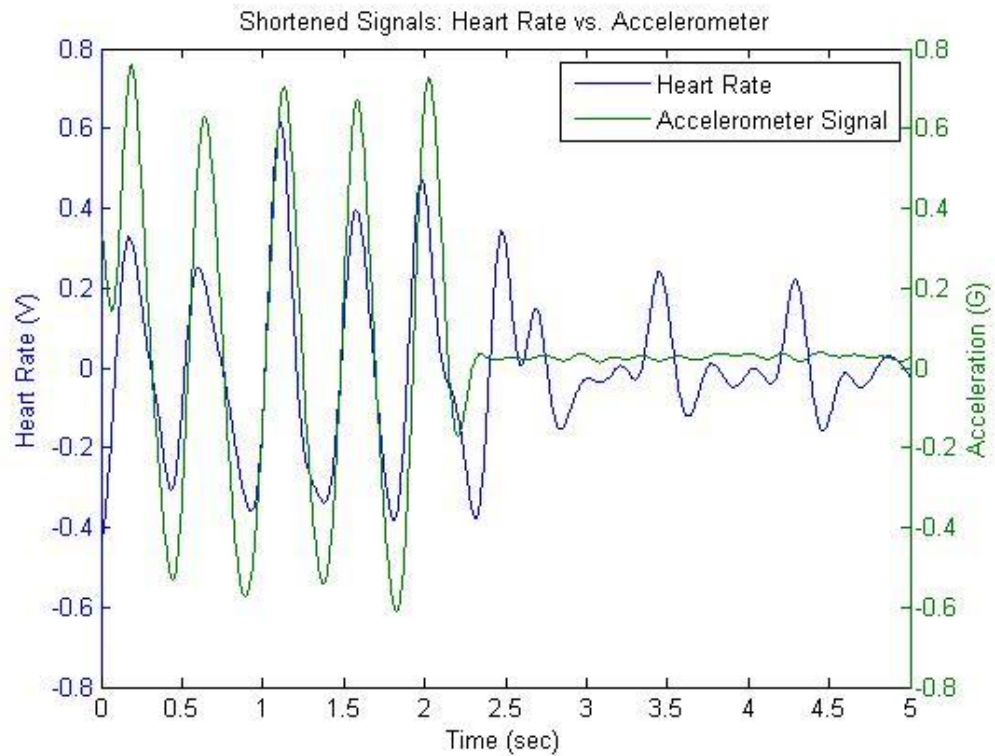


Figure 5-8: The original 5 second window that is going to be filtered

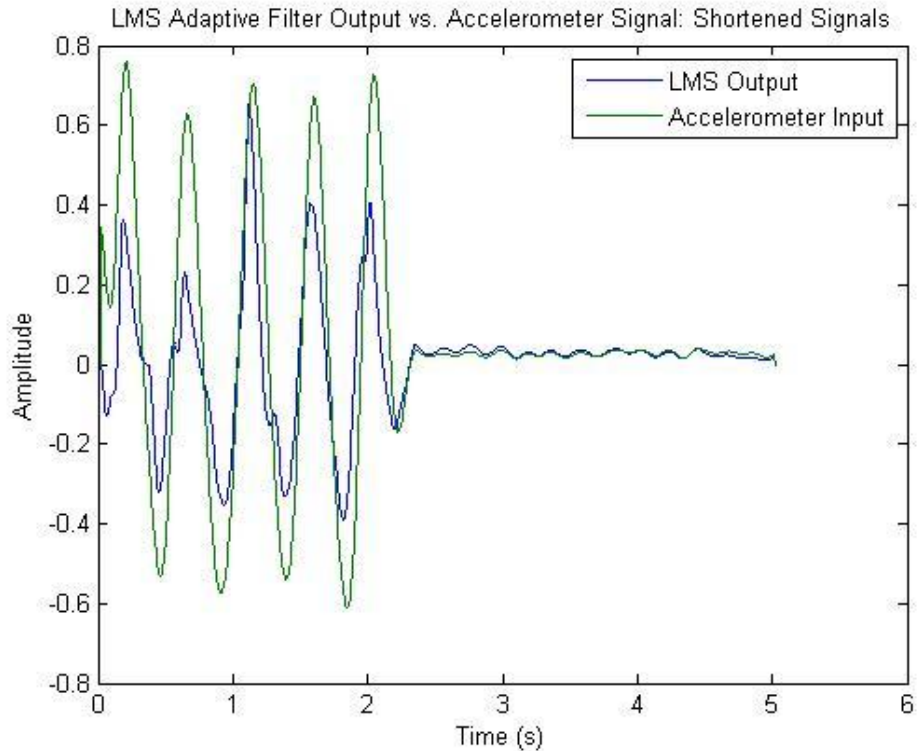


Figure 5-9: LMS Output signal vs. Accelerometer Signal

Figure 5-9 shows the LMS output for the five second window compared to the original accelerometer signal. The output of the filter should closely resemble the accelerometer input signal. It can be seen that this is the case. The two signals have a maximum normalized correlation of 0.8929, suggesting a high similarity. Figure 5-10 shows the error signal that is output from the LMS filter. This error signal should be the reconstructed heart rate signal that is void of the motion artifact. The signal is void of much of the noise but it does not appear to have a fully reconstructed heart rate signal. There are three peaks remaining; however, these peaks also occur at the same time as the peaks in the corrupted heart rate signal meaning that they cannot reasonably be used to calculate an accurate heart rate. This is representative of the LMS filter for much of the wrist sensor data. It should be noted that these signals are shifted only for appearance.

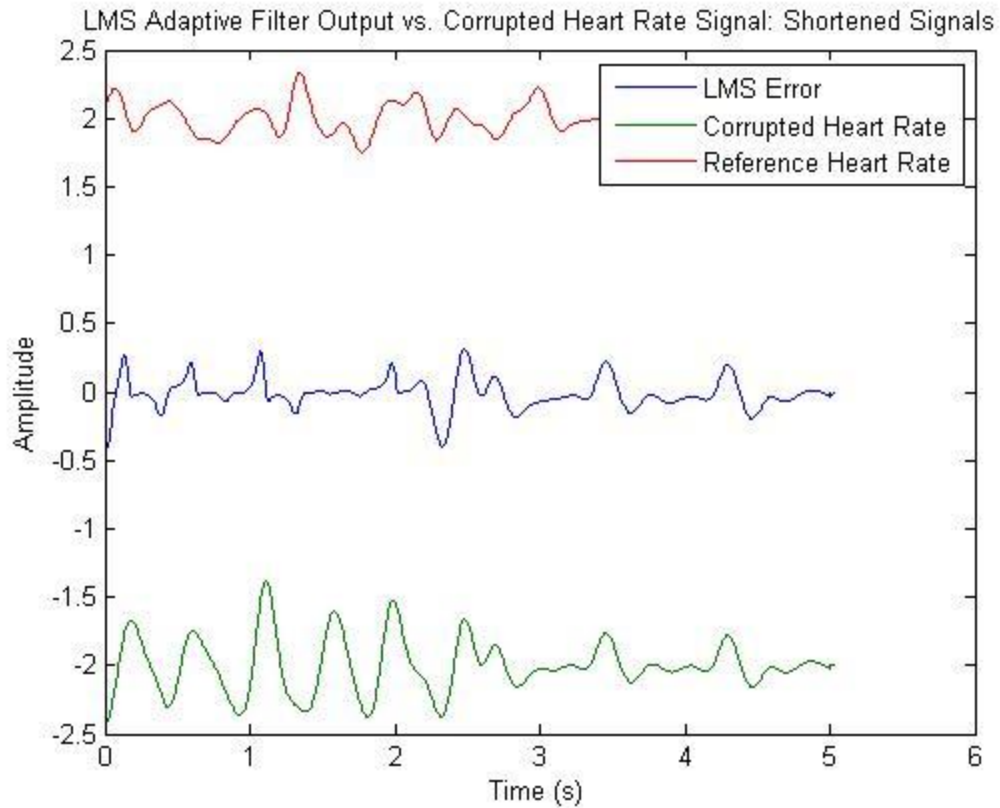


Figure 5-10: LMS Filter Error signal compared to the original heart rate signal and the reference heart rate signal

The signals in Figure 5-8 were also filtered using an RLS adaptive filter. These results are shown below. This is once again a representative data set. Figure 5-11 shows the RLS adaptive filter output signal, which should resemble the acceleration signal, just as the output of the LMS filter does. These two signals have a correlation of 0.8834, which is very similar to the output of the LMS filter.

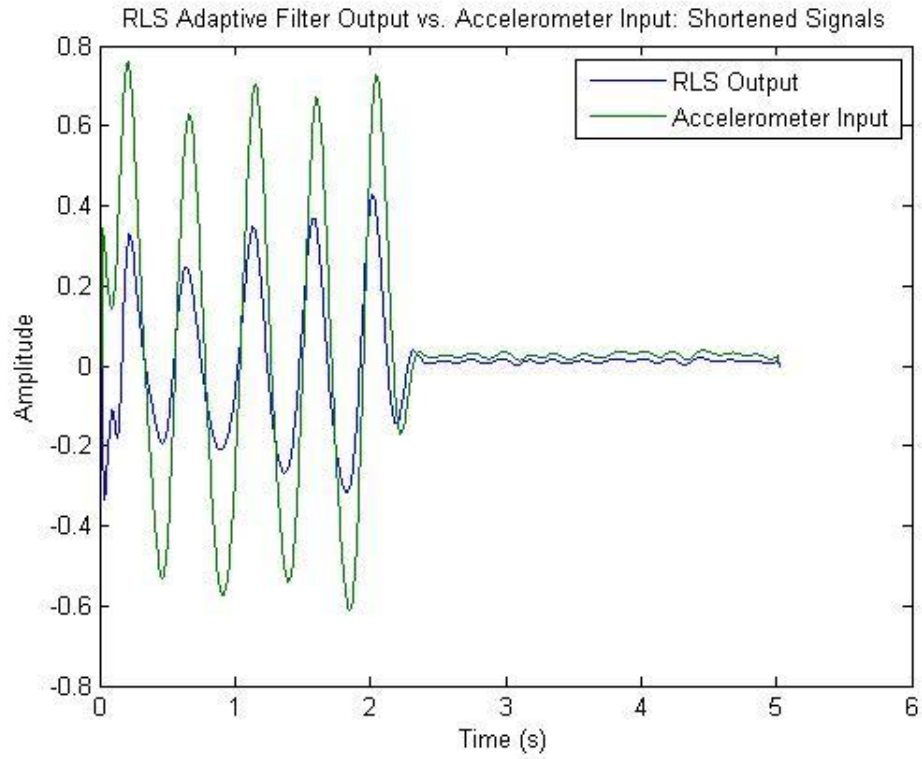


Figure 5-11: RLS output signal vs. the original accelerometer signal

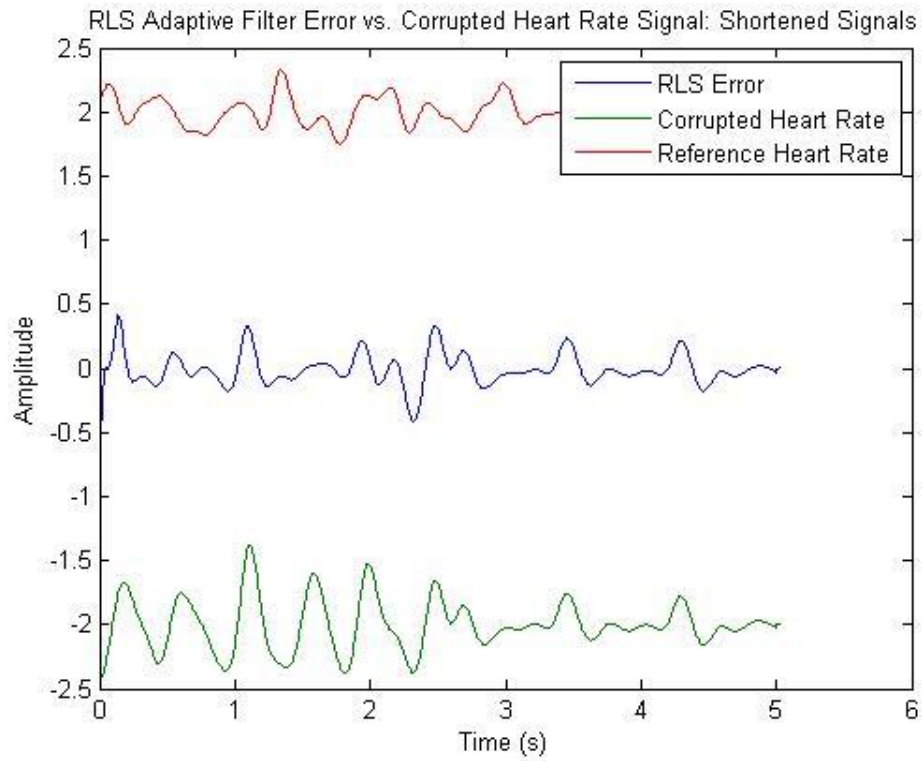


Figure 5-12: RLS Adaptive filter error output vs. the heart rate signals

Figure 5-12 shows the RLS adaptive filter error output, which should be the reconstruction of an uncorrupted heart rate signal, just as the error signal for the LMS filter was. It is evident that the error signal is void of much of the noise, but once again, it is difficult to determine a heart rate from this signal. Figure 5-13 shows the power spectrum of all the signals. The accelerometer has the most power in it and is at the same frequency as the corrupted heart rate signal, at just over 2 Hz. In both reconstructed signals, labeled as RLS reformation and LMS reformation, a new frequency begins to present itself but has a significantly lower power than that of the original signals.

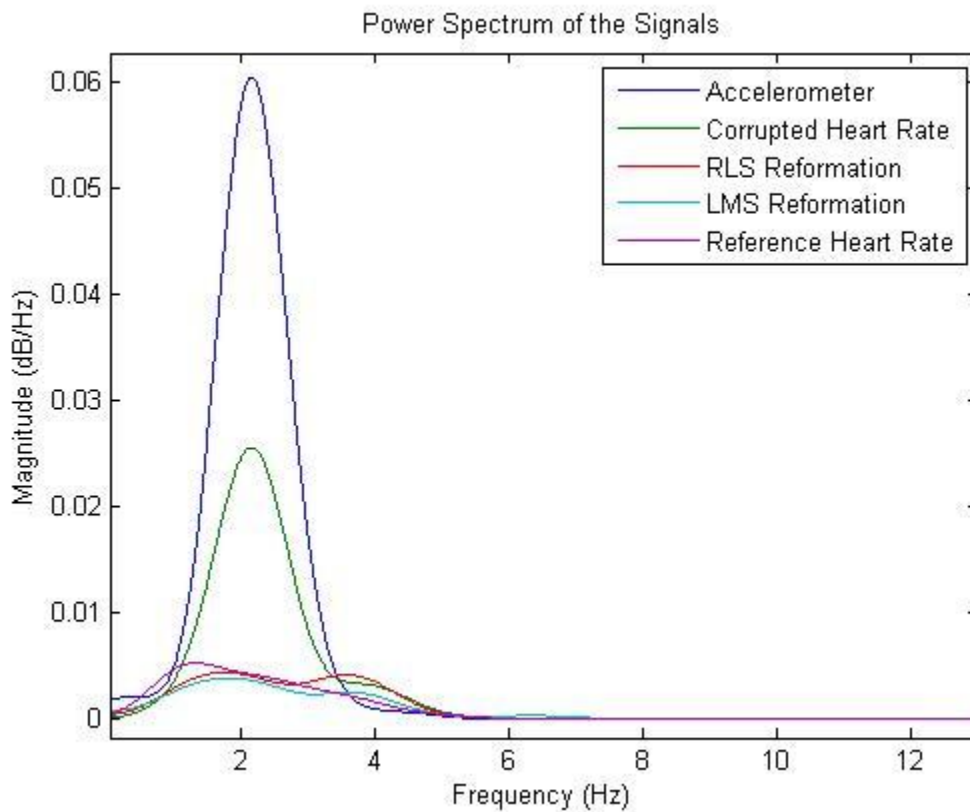


Figure 5-13: Power spectrum of the signals

5.3.2 Ring Sensor Filter Results

Below are the plots of the data sets from the ring finger that had the best correlation and resulting LMS and RLS filter results. These are representative of how the filters functioned for the majority of data sets. Figure 5-14 shows the five second window that will be sent through the LMS and RLS filters. These signals were acquired from the ring sensor placed on the left ring finger, with the accelerometer sitting on top of the hand. It can easily be seen that there is a high correlation between the heart rate and accelerometer signal.

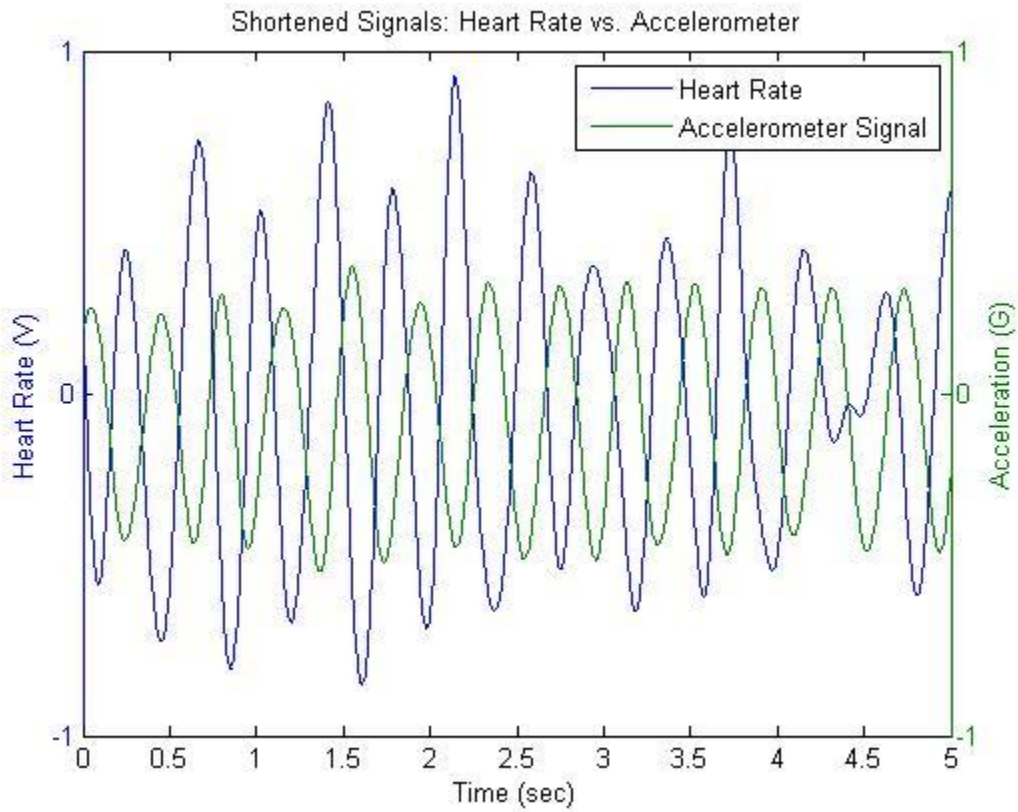


Figure 5-14: Original 5 second window for the ring sensor

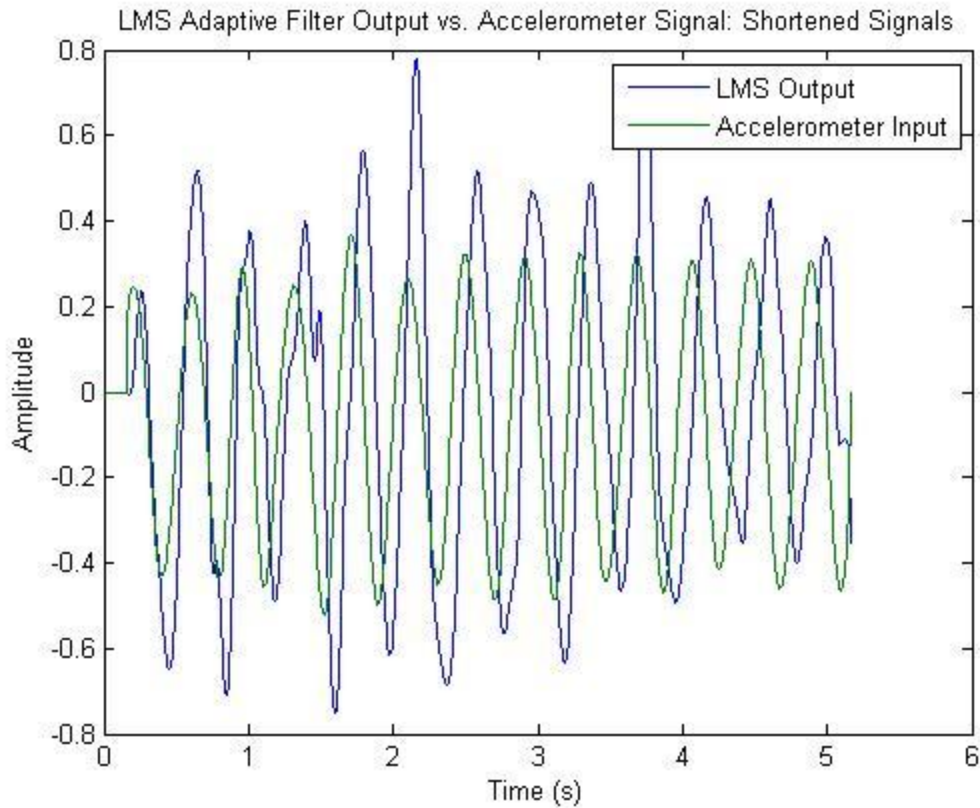


Figure 5-15: LMS output signal vs. original accelerometer signal

Figure 5-15 shows the LMS output for the five second window. The output of the filter should closely resemble the accelerometer input signal. It can be seen that this is the case. The two signals have a maximum normalized correlation of 0.7217, suggesting a high similarity. Figure 5-16 shows the error signal that is output from the LMS filter. This error signal should be the reconstructed heart rate signal minus the motion artifact. It can be seen that the signal is void of much of the noise but it does not appear to have a fully reconstructed heart rate signal. The peaks in the reconstructed signal occur at the same time as peaks in the corrupted signal and there are sections with no peaks. This is representative of the LMS filter for much of the ring sensor. It should be noted that these signals are shifted only for appearance.

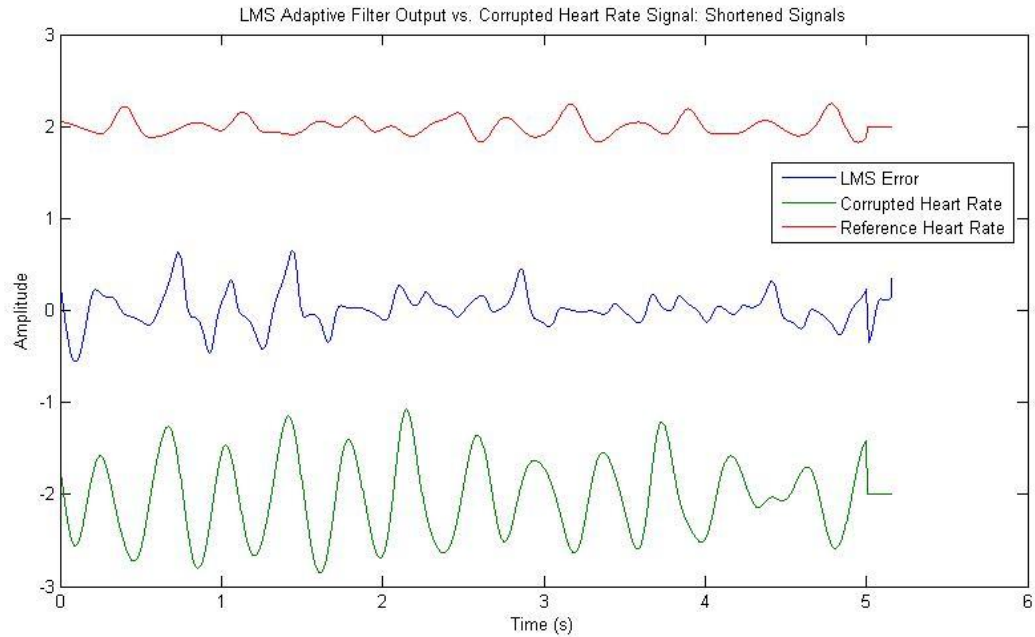


Figure 5-16: LMS filter error signal compared to the original corrupted heart rate signal

The signals in Figure 5-14 were also filtered using an RLS adaptive filter. These results are shown below. Figure 5-17 shows the RLS adaptive filter output signal, which should resemble the acceleration signal, just as the output of the LMS filter does. These two signals have a correlation of 0.8161.

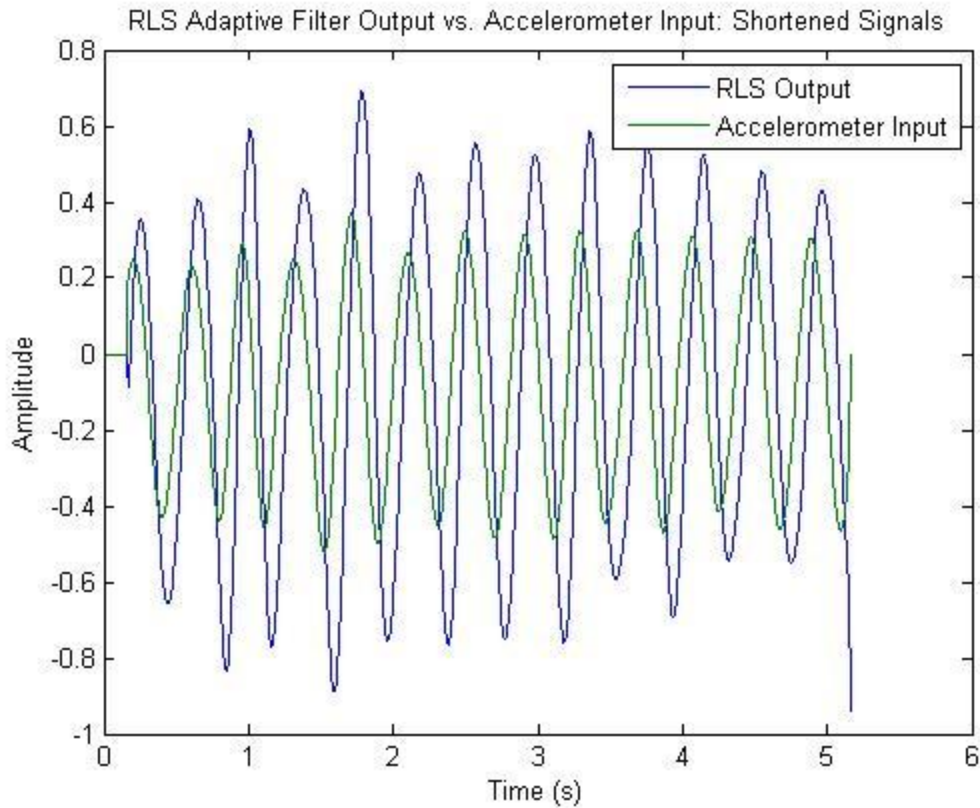


Figure 5-17: RLS output signal vs. the original accelerometer signal

Figure 5-18 shows the RLS adaptive filter error output. It is less evident in this reconstruction that the error signal is void of interference. The noise was not cancelled as well as in the LMS output and it is still difficult to discern an actual heart rate value.

Figure 5-19 shows the power spectrum of all the signals. The corrupted heart rate has the most power in it and is at the same frequency as the accelerometer signal, at just over 2 Hz. In both reconstructed signals, labeled as RLS reformation and LMS reformation, a new frequency begins to present itself but has a significantly lower power than that of the original signals.

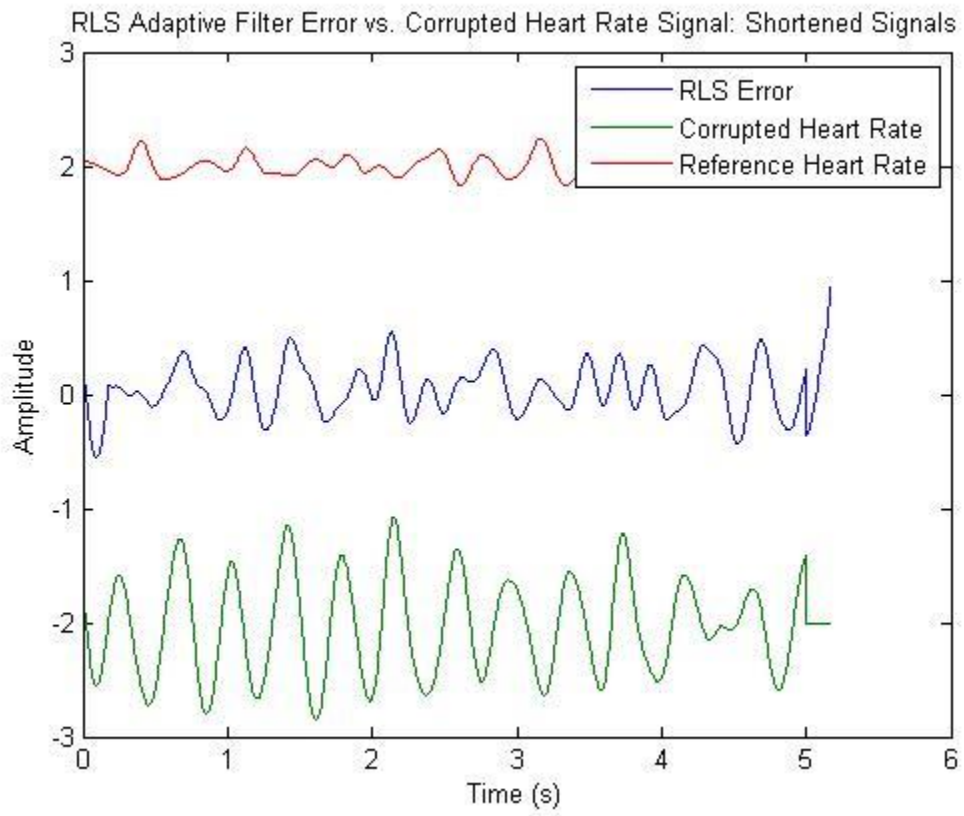


Figure 5-18: RLS filter error signal compared to the original corrupted heart rate signal

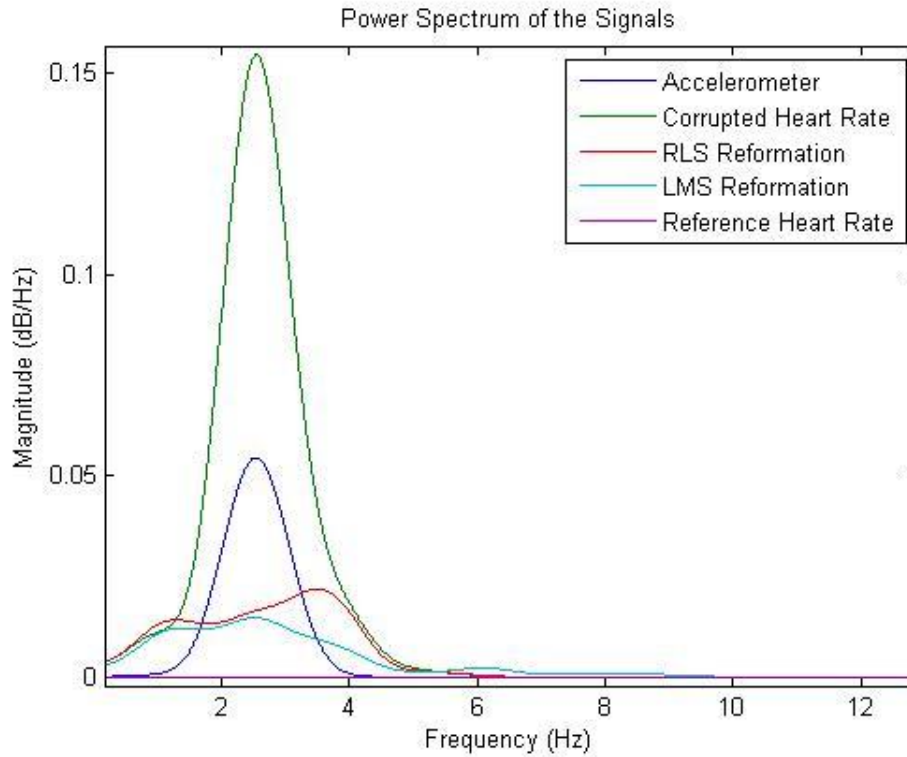


Figure 5-19: Power spectrum of the signals

5.3.3 Wrist Sensor and Ring Sensor Comparison

Once the data sets were all collected, a data analysis was performed. The root mean square of the mean of each signal was calculated. This will determine if the noise was significantly cancelled. The mean correlation of the output and error signals to the accelerometer and heart rate signals was also calculated. This data is shown in Table 5-3. For the standard deviation and error column, the values that are italicized, the RMS calculations, are standard error calculations. The other calculations in that column are standard deviations. They are standard error because the RMS calculations are averages of averages. The lower sample sizes for the correlation of the error signal to the reference signal is due to a lack of a reference signal for some of the data sets. The ring sensor

showed high correlations for both the LMS and RLS filter outputs. It also had lower standard deviations than the wrist sensor in three of the four correlation calculations.

Table 5-3: Data Summary for LMS and RLS filters across the wrist and ring sensors

		Wrist Sensor			Ring Sensor		
		Value	Standard Deviation or Error	Sample Size	Value	Standard Deviation or Error	Sample Size
LMS Adaptive Filter	RMS Mean of Heart Rate	0.3460	<i>0.0080</i>	18	0.4240	<i>0.0651</i>	11
	RMS mean of Filter Reconstruction	0.1726	<i>0.0136</i>	18	0.2096	<i>0.0362</i>	11
	Correlation: Output to Accelerometer	0.6737	0.1882	18	0.7317	0.1036	11
	Correlation: Error to reference	0.3430	0.1008	11	0.3808	0.0759	3
RLS Adaptive Filter	RMS Mean of Heart Rate	0.3460	<i>0.0080</i>	18	0.4240	<i>0.0651</i>	11
	RMS mean of Filter Reconstruction	0.2584	<i>0.0238</i>	18	0.2905	<i>0.0381</i>	11
	Correlation: Output to Accelerometer	0.8128	0.1609	18	0.8750	0.0700	11
	Correlation: Reconstruction to Reference	0.3882	0.1008	11	0.4079	0.1172	3

6 DISCUSSION AND CONCLUSION

6.1 Correlation

As can be seen in Table 5-1 and Table 5-2, there are windows of five seconds in which the heart rate signals have relatively high correlations to the accelerometer signals. This is a positive step and one of the most important ones. If the signals are not correlated, the motion would not be able to be cancelled using adaptive filtering. This step also helps determine the delay between the motion and the appearance of the resulting artifact in the heart rate signal. Without this information, the filtering would be much more difficult and likely less successful.

While correlations were high at both the wrist and the ring, there was another important discovery made. Motion in any direction at the wrist created significant interference in the heart rate signal, as demonstrated in Figure 5-2 through Figure 5-4. This was not the case for the ring sensor. Figure 5-5 shows that the ring sensor location is significantly less susceptible to motion that is not in parallel with the digital artery. It would likely be useful to research this more and possibly develop a device that was to fit on the finger like a ring and wirelessly transmit heart rate information.

6.2 Filtering

Despite the relatively high correlation between the motion artifact and the acceleration signal, the use of adaptive filters with the device yielded mixed results. For many of the data sets, the filter was able to match the acceleration signal in the heart rate and remove a portion of this signal. This is seen by the representative plots of outputs and power spectrums in Section 5.3. The power in the filter reconstructions is significantly lower

than acceleration and corrupted heart rate signals. This is also represented in Table 5-3. The root mean squares of the mean of each signal are lower in both filter outputs. In general, the LMS filter was able to remove more of the noise, with each root mean square being lower than the equivalent RLS value. The standard error is also lower in the LMS results than it is in the RLS results. These two results were true across both the wrist and ring sensors. The correlation between the output signals of the filter and the input signals of the filter were also higher in the ring sensor than the wrist sensor. This held true for the output to acceleration correlation as well as the error, or reconstruction, to reference signal correlation. However, it should be noted that the ring sensor had far fewer samples for the reference correlation than did the wrist sensor. This is also true for the general sample size.

Despite the noise removal being successful, there was not a definitive heart rate signal left. This could be due to a variety of reasons. The first, and possibly most likely, is that the harmonics of the accelerometer and corrupted heart rate signals were too similar and when cancelling the noise from the accelerometer the true heart rate signal was also largely cancelled. It is well known that the heart rate lies in the 0 to 3 Hz range, with the upper end leading to a heart rate of 180 beats per minute. As seen in Figure 5-13 and Figure 5-19, the majority of the power of both the corrupted heart rate and the accelerometer lie in very similar frequency range, both around 2 Hz. Levi Wood discusses this and the effect of human rhythms aligning with the rhythmic motion of the body, in this case the arm (21). He proposes a filter model that uses Symmetric Adaptive

Decorrelation, which can be implemented using either a standard LMS or RLS algorithm (21). He performed this using a ring sensor.

This research has determined that adaptive filtering may be a viable technique for cancelling motion artifact in a pulse oximeter signal. However, further research is needed to develop a more robust algorithm that can successfully recover a heart rate, even if its harmonics correspond to the harmonics that are present in the accelerometer signal.

6.3 Future Work

The development of a ring sensor would be a useful step for future work. It was determined that the ring sensor would require fewer degrees of freedom due to its insusceptibility to motion in two axes. This does not hold true to the wrist sensor, which was affected by motion in any axis. Another future step would be to further investigate the methods performed by Wood. By using a technique that better accounts for the correlation and similar harmonics, he was successful in reconstructing a heart rate signal that was not only accurate in frequency but also in amplitude. This would be vital if the sensor were ever to be used as a true pulse oximeter to detect oxygen saturation, as amplitude of the signal has a significant role in its calculation.

There are a few other paths that could be taken in the future as well. The first is collecting data at a higher sampling rate so that it would be more plausible to use a higher filter order. As discussed in Section 4.5.4, the sampling rate used is high enough. However, the filter length does not allow for a high enough filter resolution. In order to gain a higher resolution, the filter length must be increased, which increases computational time. By

sampling at a higher frequency, the time the filter takes to converge will decrease. The second path is using different filtering techniques, including non-linear filters, such as Volterra series, Kalman filters, and principal component analysis. These types of filters have been used in other studies and may provide a better approach than LMS and RLS adaptive filtering, as some would allow for the assumptions discussed in Section 4.5.3 to be violated. For example, the Volterra series filter is a non-linear filter and would account for motion that causes a non-linear response in the heart rate signal.

7 WORKS CITED

1. *Comparison of Two Pulse Oximeters During Sub-maximal Exercise In Healthy Volunteers: Effects of Motion.* **Kist, William.** 2002, Journal of Exercise Physiology.
2. *Signal Processing Methods for Pulse Oximetry.* **Rusch, T.L.** 2, March 1996, Computers in Biology and Medicine, Vol. 26.
3. **Hall, John E. and Guyton, Arthur.** *Guyton and Hall Textbook of Medical Physiology.* Philadelphia : Saunders Elsevier, 2010.
4. *A Review of the Principles of Pulse Oximetry and Accuracy of Pulse Oximeter Estimates During Exercise.* **Mengelkoch, Larry J.** 1, January 1994, Physical Therapy, Vol. 74.
5. **Dresher, Russell.** *Wearable Forehead Pulse Oximetry: Minimization of Motion and Pressure Artifacts.* 2006. Masters Thesis.
6. *Pulse Oximetry: Its invention, theory, and future.* **Aoyagi, Takuo.** 2003, Journal of Anesthesia.
7. *Pulse Oximetry: Theory and Applications for Noninvasive Monitoring.* **Mendelson, Yitzhak.** 9, 1992, Clinical Chemistry, Vol. 38.
8. *The Effect of Motion on Pulse Oximetry and Its Clinical Significance.* **Petterson, Michael T.** 6, 2007, Anesthesia & Analgesia, Vol. 105.
9. *Accuracy of Pulse Oximetry During Exercise Stress Testing.* **Norton, L.H.** 7, 1992, International Journal of Sports Medicine, Vol. 13.
10. *A New Method for Pulse Oximetry Possessing Inherent Insensitivity to Artifact.* **Hayes, Matthew James and Smith, Peter R.** 3, April 2001, IEEE Transactions on Biomedical Engineering, Vol. 48.
11. *Artifact Reduction in Photoplethysmography.* **Hayes, Matthew James and Smith, Peter R.** 31, November 1998, Optical Society of America, Vol. 37.
12. *Motion Artifact Cancellation in NIR Spectroscopy Using Discrete Kalman Filtering.* **Izzetoglu, Meltem.** 2010, Biomedical Engineering Online.
13. *Motion Artifact Cancellation in NIR Spectroscopy Using Wiener Filtering.* **Izzetoglu, Meltem.** 5, May 2005, IEEE Transactions on Biomedical Engineering, Vol. 52.
14. *Reduction of Motion Artifact in Pulse Oximetry by Smoothed Pseudo Wigner-Ville Distribution.* **Yan, Yong-sheng.** 3, March 2005, Journal of NeuroEngineering and Rehabilitation, Vol. 2.
15. *An Efficient Motion-Resistant Method of Wearable Pulse Oximeter.* **Yan, Yong-sheng.** 3, May 2008, IEEE Transactions on Information Technology in Biomedicine, Vol. 12.
16. *Reducing Motion Artifact in Wearable Biosensors Using MEMS Accelerometers for Active Noise Cancellation.* **Gibbs, Peter.** Portland, OR : s.n., 2005. American Control Conference.
17. **Jones, Douglas L.** Adaptive Filtering: LMS Algorithm. *Connexions.* [Online] June 2009. <http://cnx.org/content/m10481/latest/>.
18. **Semmlow, John L.** *Biosignal and Medical Image Processing.* 2. Boca Raton : CRC Press, 2009.
19. *Wavelets for Biomedical Signal Processing.* **Akay, Metin.** Chicago, IL : s.n., 1997. IEEE/EMBS.

20. *Implementation of ECG Signal Processing and Analysis Techniques in Digital Signal Processor based System.* **Balasubramaniam, D.** Cetraro, Italy : s.n., 2009. International Workshop on Medical Measurements and Applications.
21. *Active Motion Artifact Reduction for Wearable Sensors Using Laguerre Expansion and Signal Separation.* **Wood, Levi.** Shanghai, China : s.n., 2005.
22. *Heart Rate Monitoring via Remote Photoplethysmography With Motion Artifacts Reduction.* **Cennini, Giovanni.** 5, 2010, Optics Express, Vol. 18.

APPENDIX A: MATLAB CODE

```
% Chris Dickson
% Thesis: Heart Rate Artifact Suppression

clear all;
close all;

HR = load('HRdata.txt');
X = load('accelX.txt');
Y = load('accelY.txt');
Z = load('accelZ.txt');

HR2 = load('HRdata2.txt');
%HR2 = zeros(length(HR),1);
HR = HR(length(HR)-length(X)+1:end);
t = 0:(1/240):(length(HR)/240)-(1/240);
figure();
plot(t, X, t, Y, t, Z, t, HR);
legend('X', 'Y', 'Z', 'HR');

start = 10;
HR = HR(start*240:end);
X = X(start*240:end);
Y = Y(start*240:end);
Z = Z(start*240:end);
HR2 = HR2(start*240:end);

t = 0:(1/240):(length(HR)/240)-(1/240);
% figure();
% plot(t, X, t, Y, t, Z, t, HR);
% xlabel('Time (sec)');
% ylabel('Amplitude');
% legend('X-axis', 'Y-axis', 'Z-axis', 'Heart Rate');
% title('Original Plots of Heart Rate and Accelerometer Signals');

FsHR = 240;
N = length(HR);FsHR = 240;
nyquistFreq = FsHR/2;
NFFT = 2^nextpow2(N);

nyquistFreqHR = FsHR/2;

% run accel signal through low pass filter
WnHR = 5/nyquistFreqHR;
% need an order of 100
filt1 = fir1(100, WnHR);
```

```

t = (1:N)/FsHR;

X = filter(filt1, 1, X);
Y = filter(filt1, 1, Y);
Z = filter(filt1, 1, Z);
HR = filter(filt1, 1, HR);
HR2 = filter(filt1, 1, HR2);

% Zero mean
HRzero = HR - mean(HR);
Xzero = X - mean(X);
Yzero = Y - mean(Y);
Zzero = Z - mean(Z);
HR2zero = HR2 - mean(HR2);

% Calculate the unit signals for each (volts for HR, G's for accel)
HRv = HRzero.*(3/1024);
Xg = Xzero .*(8/1024);
Yg = Yzero.*(8/1024);
Zg = Zzero.*(8/1024);
HR2v = HR2zero.*(3/1024);

figure();
subplot(2,1,1); plot(t, HRv);
xlabel('Time (sec)');
ylabel('Voltage (V)');
legend('Corrupted Heart Rate');
title('Heart Rate Signals');
subplot(2,1,2); plot(t, Zg);
xlabel('Time (sec)');
ylabel('Acceleration (G)');
legend('Z-Axis of Accelerometer');
title('Accelerometer Signal');

%%

% accelerometer signal with the most motion
accel = Yg;

maxCorr = 0;
step = 5; % number of seconds to increment the window
start = 0;
stop = step;
maxStart = 0;
maxIndex = 0;

% determine when the motion stops and starts again
% there are periods of motion and no motion in each set, just want to look
% at periods of motion
noMotionIndex = 123;

```

```

motionStart = 171;
noMotionIndex2 = 0;
motionStart2 = 0;
noMotionIndex3 = 0;
motionStart3 = 0;
motionStop = 216;

% Find the 5 second window with the highest correlation
while stop <= (length(Xg)/240)

    accelShort = accel((start*240)+1:(stop*240));
    HRshort = HRv((start*240)+1:(stop*240));
    [corrM, lagsShort] = xcorr(accelShort,HRshort, 'coeff');
    corrM = corrM((length(accelShort)):end);
    lagsShort = lagsShort((length(accelShort)):end);
    [corr, i] = max(corrM);

    if(corr > maxCorr)
        maxCorr = corr;
        lags = lagsShort;
        corrShort = corrM;
        maxStart = start;
        maxIndex = i;
    end

    start = start + 0.1;
    stop = start + step;
    if (start >= noMotionIndex) && (start <= motionStart)
        start = motionStart;
        stop = start + step;
    end
    if (stop > noMotionIndex) && (stop <= motionStart)
        start = motionStart;
        stop = start + step;
    end
    if (start >= noMotionIndex2) && (start <= motionStart2)
        start = motionStart2;
        stop = start + step;
    end
    if (stop > noMotionIndex2) && (stop <= motionStart2)
        start = motionStart2;
        stop = start + step;
    end
    if (start >= noMotionIndex3) && (start <= motionStart3)
        start = motionStart3;
        stop = start + step;
    end
    if (stop > noMotionIndex3) && (stop <= motionStart3)
        start = motionStart3;
        stop = start + step;
    end
end

accelShort = accel((maxStart*240)+1:(maxStart*240)+(step*240));
HRvshort = HRv((maxStart*240)+1:(maxStart*240)+(step*240));
HR2vshort = HR2v((maxStart*240)+1:(maxStart*240)+(step*240));

```

```

% Plot the correlation of the 5 second window
lagsS = lags./240;
figure();
plot(lagsS, corrShort);
xlabel('Lag Time (sec)');
ylabel('Correlation');
title('Correlation of the Accelerometer to the Heart Rate');

% calculate teh correlation for the full signals
% this calculation is likely not useful
d = abs(lags(maxIndex));
d = d+1;
maxIndexShort = maxIndex/240;
[corrFull, lagsFull] = xcorr(accel, HRv, 'coeff');
corrFull = corrFull(length(accel):end);
lagsFull = lagsFull(length(accel):end);
[maxCorrFull, iFull] = max(corrFull);
maxIndexFull = (lagsFull(iFull)/240);

% zero pad the signals to account for the delay prior to sending through
% the filters
zeropad = zeros(d,1);
HRpad = padarray(HRvshort, [d 0]);
HRpad = HRpad(d:end);
accelPad = padarray(accelShort, [d 0]);
accelPad = accelPad(1:(end-d+1));
HR2pad = padarray(HR2vshort, [d 0]);
HR2pad = HR2pad(d:end);

% get the RLS filter
order = 10;
l = order+1;      % filter length
lambda = 1;      % RLS forgetting factor
invcov = 10*eye(l);
coeffs = [];
states = [];
RLSfilt = adaptfilt.rls(l, lambda, invcov);

% get the LMS filter
l = order;
step = 0.15; %0.5 good, 0.15 good, 0.7 too high
leak = 0.5;
coeffs = [];
states = [];
LMSfilt = adaptfilt.lms(l, step);

[outRLSshort, errorRLSshort] = filter(RLSfilt, accelPad, HRpad);
[outRLS, errorRLS] = filter(RLSfilt, accel, HR);

[outLMSshort, errorLMSshort] = filter(LMSfilt, accelPad, HRpad);
[outLMS, errorLMS] = filter(LMSfilt, accel, HR);

% compute the maximum correlation of the outputs and inputs for both

```

```

% fitlers
accelRLScorr = max(xcorr(outRLSshort, accelPad, 'coeff'));
accelLMScorr = max(xcorr(outLMSshort, accelPad, 'coeff'));
errorRLScorr = max(xcorr(errorRLSshort, HR2pad, 'coeff'));
errorLMScorr = max(xcorr(errorLMSshort, HR2pad, 'coeff'));

% compute the RMS value for the signals (error signal)
rmsErrorRLS = sqrt(mean(errorRLSshort.^2));
rmsErrorLMS = sqrt(mean(errorLMSshort.^2));
rmsHR = sqrt(mean(HRpad.^2));
rmsHR2 = sqrt(mean(HR2pad.^2));

% compute the frequency power spectrum of it (power should be lower at
% harmonic of the accelerometer
% show before and after
[powAccel, freqAccel] = pwelch(accelPad, [], [], NFFT, FSHR);
[powHR, freqHR] = pwelch(HRpad, [], [], NFFT, FSHR);
[powRLS, freqRLS] = pwelch(errorRLSshort, [], [], NFFT, FSHR);
[powLMS, freqLMS] = pwelch(errorLMSshort, [], [], NFFT, FSHR);
[powHR2, freqHR2] = pwelch(HR2pad, [], [], NFFT, FSHR);

% Plor the power spectrums of the signals
figure();
plot(freqAccel, powAccel, freqAccel, powHR, freqAccel, powRLS, freqAccel,
powLMS, freqAccel, powHR2);
legend('Accelerometer', 'Corrupted Heart Rate', 'RLS Reformation', 'LMS
Reformation', 'Reference Heart Rate');
xlabel('Frequency (Hz)');
ylabel('Magnitude (dB/Hz)');
title('Power Spectrum of the Signals');

%%

% Signal Plots
tshort = 0:(1/240):(length(accelShort)/240)-(1/240);
figure();
[AX, H1, H2] = plotyy(tshort, HRvshort, tshort, accelShort, 'plot');
set(get(AX(1), 'Ylabel'), 'String', 'Heart Rate (V)')
set(get(AX(2), 'Ylabel'), 'String', 'Acceleration (G)')
xlabel('Time (sec)');
legend('Heart Rate', 'Accelerometer Signal');
title('Shortened Signals: Heart Rate vs. Accelerometer');

tpad = 0:(1/240):(length(accelPad)/240)-(1/240);
figure();
[AX, H1, H2] = plotyy(tpad, HRpad, tpad, accelPad, 'plot');
set(get(AX(1), 'Ylabel'), 'String', 'Heart Rate (V)')
set(get(AX(2), 'Ylabel'), 'String', 'Acceleration (G)')
legend('Heart Rate', 'Accelerometer Signal');
title('Shortened Plots: Zero-padded');

% RLS plots
figure();
plot(tpad, outRLSshort, tpad, errorRLSshort);

```

```

xlabel('Time (s)');
ylabel('Amplitude');
legend('RLS Output', 'RLS Error');
title('RLS Adaptive Filter Output vs. Error: Shortened Signals');

figure();
plot(tpad, outRLSshort, tpad, accelPad);
xlabel('Time (s)');
ylabel('Amplitude');
legend('RLS Output', 'Accelerometer Input');
title('RLS Adaptive Filter Output vs. Accelerometer Input: Shortened
Signals');

tpad = 0:(1/240):(length(accelPad)/240)-(1/240);
figure();
plot(tpad, errorRLSshort, tpad, HRpad-2, tpad, HR2pad+2);
xlabel('Time (s)');
ylabel('Amplitude');
legend('RLS Error', 'Corrupted Heart Rate', 'Reference Heart Rate');
title('RLS Adaptive Filter Error vs. Corrupted Heart Rate Signal: Shortened
Signals');

% LMS Plots
figure();
plot(tpad, outLMSshort, tpad, errorLMSshort);
xlabel('Time (s)');
ylabel('Amplitude');
legend('LMS Output', 'LMS Error');
title('LMS Adaptive Filter Output vs. Error: Shortened Signals');

figure();
plot(tpad, outLMSshort, tpad, accelPad);
xlabel('Time (s)');
ylabel('Amplitude');
legend('LMS Output', 'Accelerometer Input');
title('LMS Adaptive Filter Output vs. Accelerometer Signal: Shortened
Signals');

tpad = 0:(1/240):(length(accelPad)/240)-(1/240);
figure();
plot(tpad, errorLMSshort, tpad, HRpad-2, tpad, HR2pad+2);
xlabel('Time (s)');
ylabel('Amplitude');
legend('LMS Error', 'Corrupted Heart Rate', 'Reference Heart Rate');
title('LMS Adaptive Filter Output vs. Corrupted Heart Rate Signal: Shortened
Signals');

```